Chapter 5

Application of the GEV Approach for Seismic Hazard Analysis in the Kopili Fault, Indo-Burma, and EAFZ Regions

Chapter 5

Application of the GEV Approach for Seismic Hazard Analysis in the Kopili Fault, Indo-Burma, and EAFZ Regions

5.1. Introduction

Seismic parameters play a pivotal role in understanding and mitigating the risks associated with earthquakes, especially in seismically active regions such as the Kopili Fault Region, Indo-Burma Region, and the EAFZ. These parameters provide crucial insights into the frequency, magnitude, and distribution of seismic events, empowering researchers with valuable information for infrastructure planning, disaster preparedness, and risk management strategies. Among the various methodologies employed to analyze seismic data, the GEV approach aided with b-value stands out as a robust statistical framework for modeling extreme events, including earthquakes. Originating from the field of hydrology, the Gumbel distribution has been extensively applied in seismology to estimate the maximum magnitudes and return periods of earthquakes, thereby facilitating seismic hazard assessments and engineering designs. In this chapter, we delve into the seismic parameters of the aforementioned regions using the GEV approach. Each of these regions exhibits unique tectonic settings and seismic characteristics, making them prime candidates for comprehensive seismic analysis. By applying the Gumbel methodology, the aim is to elucidate the probabilistic behavior of seismic events in these areas—offering valuable insights into the potential risks posed by future earthquakes. Through a systematic examination of historical seismic data and geophysical observations, we endeavor to quantify key seismic parameters, involving the maximum magnitude, return period, and intensity-frequency relationships. While doing so, we seek to enhance the understanding of seismic hazard dynamics in the Kopili Fault Region, Indo-Burma Region and the EAFZ. Accordingly, the following sections describe the adoption of Gumbel extreme vale approach in these regions.

5.2. Probabilistic estimation of seismic hazard attributes for Kopili region of northeast India

5.2.1. Introduction

Northeast India, spanning 89°E-98°E and 22°N-30°N, is a significant seismic zone due to diverse tectonic features (as shown in Figure 5.1). Notable earthquakes include the 1897 Shillong (M_W 8.1) and the 1950 Assam (M_W 8.7) earthquakes. The region, classified as a high seismic risk zone (zone V) with a factor of 0.36g by the [1], is unstable due to collisions between the Indian plate and Tibet and the Burmese landmass. It is divided into four seismogenic zones: eastern syntaxis, Arakan-Yoma subduction belt, Shillong plateau, and east-trending Himalayan thrust. The Shillong plateau, particularly along the Dauki and Kopili faults, is highly active, experiencing major earthquakes in 1897, 1941, 1943, and 2021. Accurate earthquake forecasting remains challenging, making seismic hazard assessment crucial. This chapter aims to delineate seismic attributes for the Kopili fault and surrounding areas, using the GEV method [2], [3].

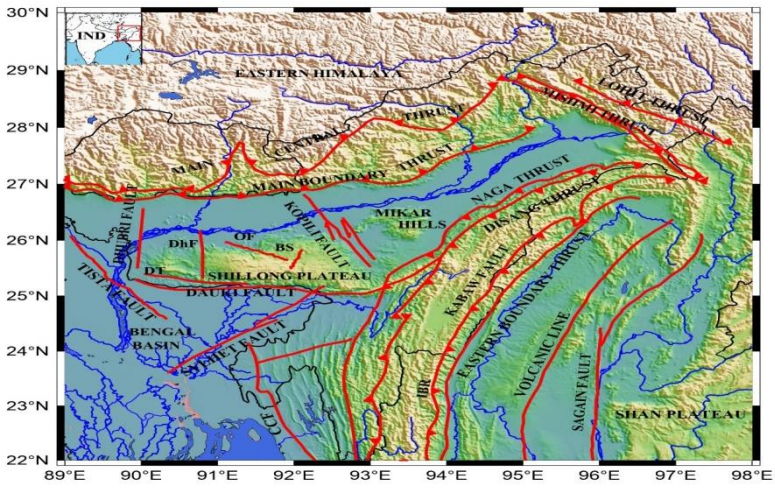

Figure 5.1. The topological plot of the NER of the Indian subcontinent shows various faults and thrusts. The prominent tectonic features in this region include; MCT, MBT, LH, MT, KF, DF, SF, DT, DhF, Dhubri fault, Tista fault, Kaladan Fault, CCF, OF, BS, NT, Kopili fault. The major thrusts located are shown by the teeth lines. Inset map showing the highlighting study region [4].

5.2.2. Tectonic setup

Figure 5.2 presents a topological map featuring the eastern Himalayan zone, Assam valley, and Shillong plateau. The Kopili fault, situated between the Shillong plateau and the Mikir hill plateau, is a major seismic feature. The Kopili fault, stretching 300 km NW-SE from Manipur to the Bhutan-Arunachal Pradesh-Assam trijunction, caused the 2009 Bhutan earthquake. This fault exhibits active seismicity, especially near its intersection with the MCT, as evidenced by the September 21, 2009 earthquake. Both events displayed shallow, right-lateral strike-slip faulting. The Kopili fault's seismogenic zone extends to about 47 km depth [5]. Figure 5.2 also indicates the epicenter of the April 28, 2021 earthquake (M_W 6.4) with yellow stars.

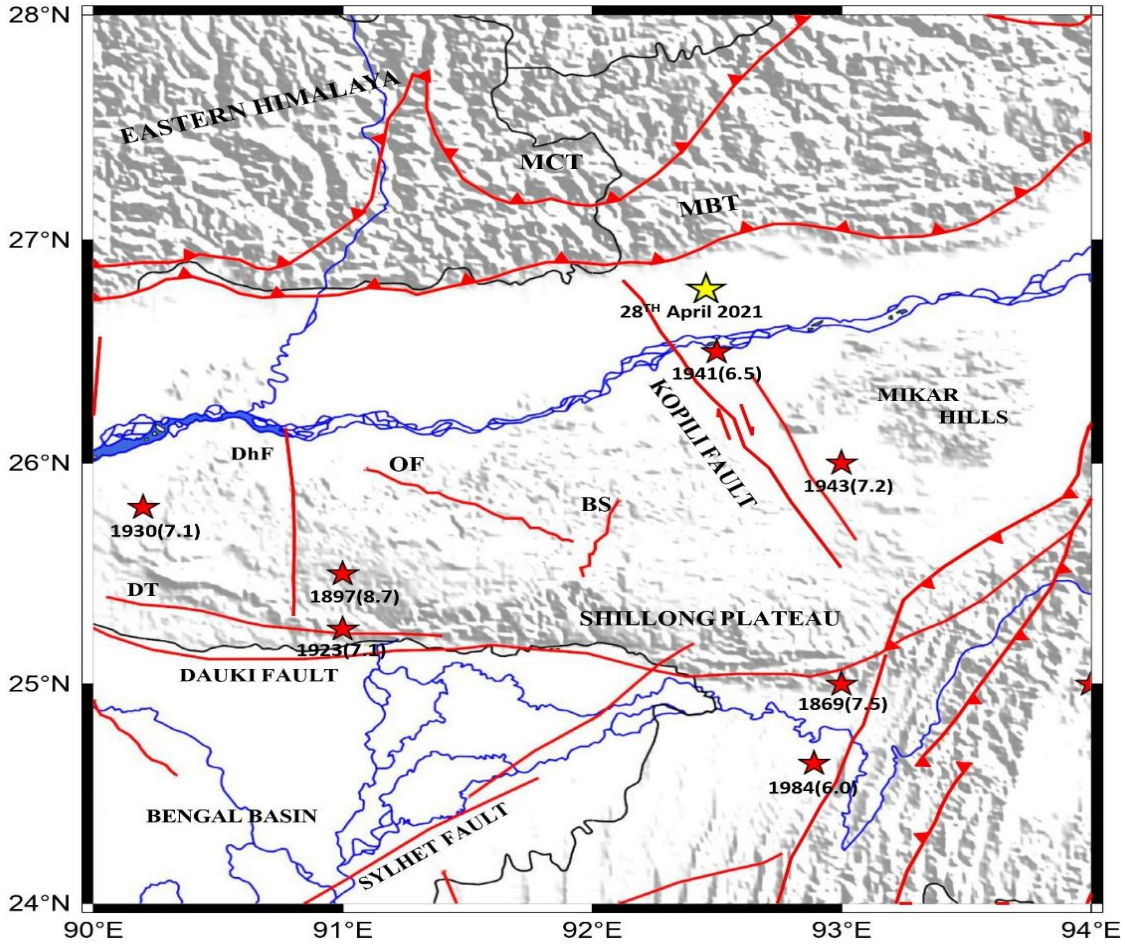

Figure 5.2: The tectonic plot of the study region. the major earthquake events that happened in this region are shown by red stars. The epicentral location 28th April 2021 earthquake is shown by the yellow star. MBT, MCT, OF, KF, NT, DF, SF, DT, DhF, BS, Kopili fault. The thrust lines are shown by the teeth lines.

5.2.3. Data Analysis

The study area (24°-28°N, 90°-94°E) includes earthquake data from 1964 to 2022, with 550 events of magnitude $M_W \geq 3.4$ from USGS and ISC databases. Data initially recorded on various scales (M_D, M_L, mb, M_S) is converted to the M_W scale for consistency and accuracy, based on [6] and [7] (as mentioned in Table 2.1 of chapter 2). Figure 5.3 shows the distribution of these events.

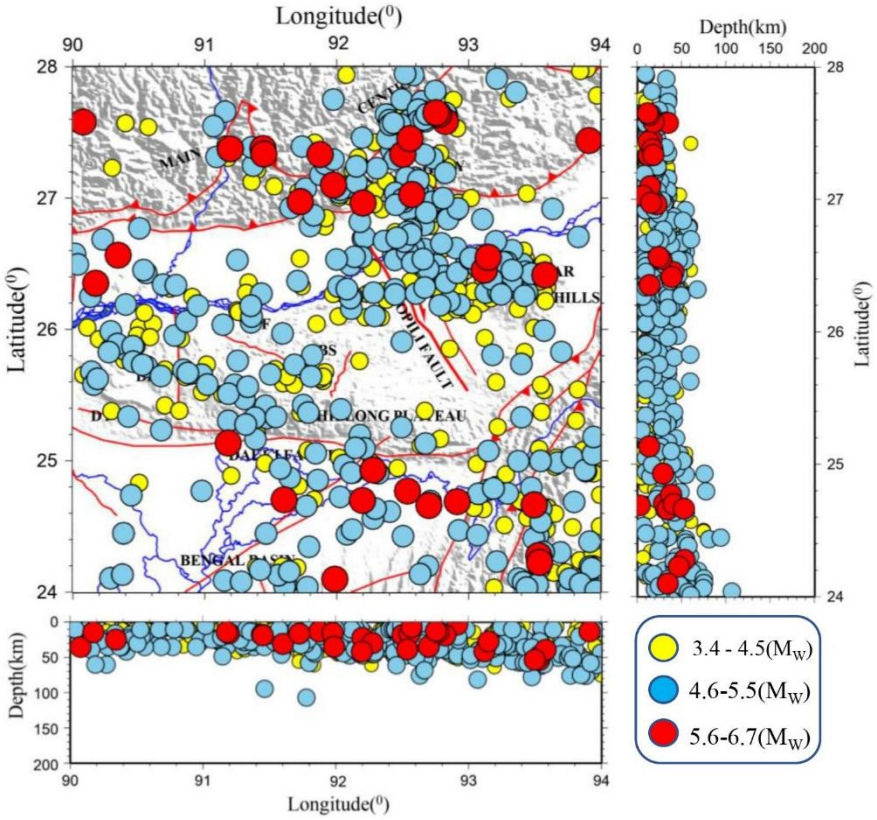

Figure 5.3: The epicentral location of all the events with magnitude Mw≥3.4.

5.2.4. Estimation of seismic hazard parameters

Extreme value theory of Gumbel

We have estimated the b-value using the Gumbel coefficients α and β for analysis. Furthermore, the data set used for the calculation of the above parameters is given in the Table 5.1 below.

Table 5.1: Estimation of parameters used for Gumbel's annual maximum distribution

Magnitude	J	f	G(m)	N = -ln(G)	Ln(-ln(G))	Log(N)
3.7	1	0.017	0.017	4.074	1.405	0.610
4.2	1	0.017	0.034	3.381	1.218	0.529
4.6	1	0.017	0.051	2.976	1.090	0.473
4.7	2	0.034	0.085	2.465	0.902	0.391
4.8	4	0.067	0.152	1.884	0.633	0.275
4.9	4	0.067	0.219	1.519	0.417	0.182
5.0	4	0.067	0.289	1.252	0.224	0.097
5.1	4	0.067	0.353	1.041	0.040	0.017
5.2	1	0.017	0.370	0.994	-0.005	-0.003
5.3	2	0.034	0.404	0.906	-0.098	-0.043
5.4	8	0.134	0.538	0.620	-0.478	-0.208
5.5	2	0.034	0.572	0.559	-0.582	-0.253
5.6	6	0.100	0.672	0.397	-0.922	-0.400
5.7	7	0.117	0.789	0.237	-1.439	-0.625
5.8	2	0.034	0.823	0.195	-1.635	-0.710
5.9	5	0.084	0.907	0.098	-2.327	-1.010
6.0	1	0.017	0.924	0.080	-2.537	-1.102
6.2	2	0.034	0.958	0.043	-3.149	-1.367
6.4	1	0.017	0.975	0.025	-3.676	-1.596
6.7	1	0.017	0.992	0.008	-4.824	-2.095

Here, Magnitude (M) is the magnitude of observed earthquake arranged in the increasing order, J gives the number of earthquake magnitude observed and f gives the relative frequency of earthquake calculated using the formula (f=J/n+1) and G(m) gives cumulative relative frequency of the earthquake.

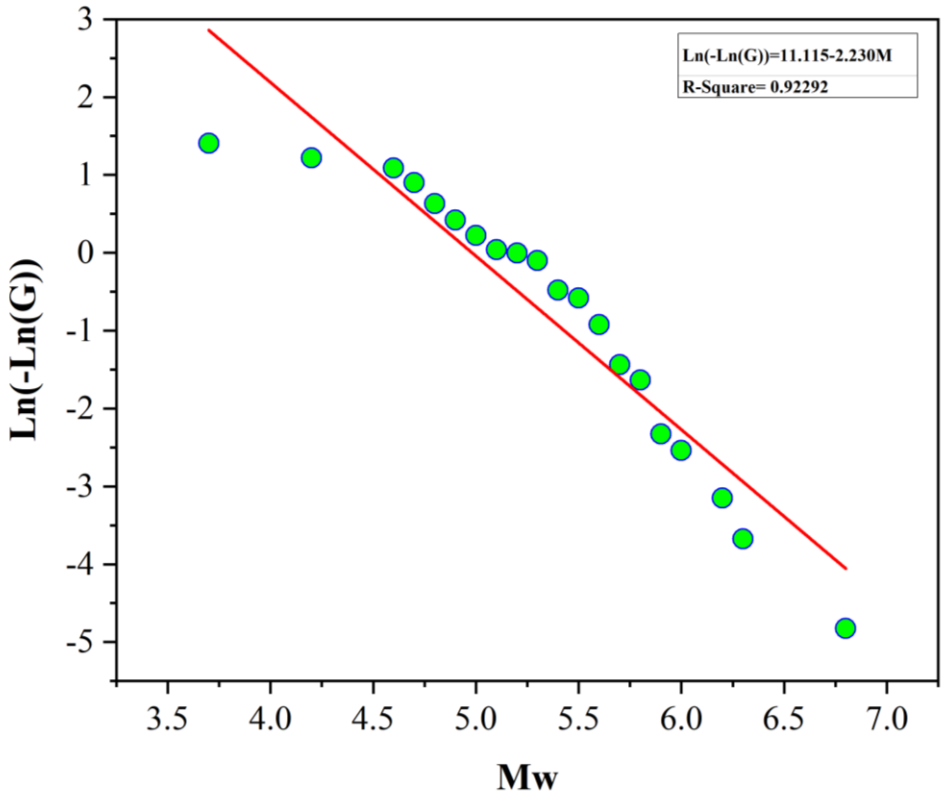

Figure 5.4: The simplified relation for estimating α and β using linear regression of data [2], [3].

Following observations are made from the above regression (figure 5.4)

$\alpha = 66988.250$, $\beta = 2.230$ and $\ln \alpha = 11.115$

Figure 5.5 shows the results of using the least square method. The regression relation determines the a and b-values for the examined region.

$\log_{10} N(m) = 4.826 - 0.970Mw$

As illustrated in Figure 5.5, the b-value derived using the Gumbel approach is 0.97, which is consistent with the average b-value of 1 for any seismically active location.

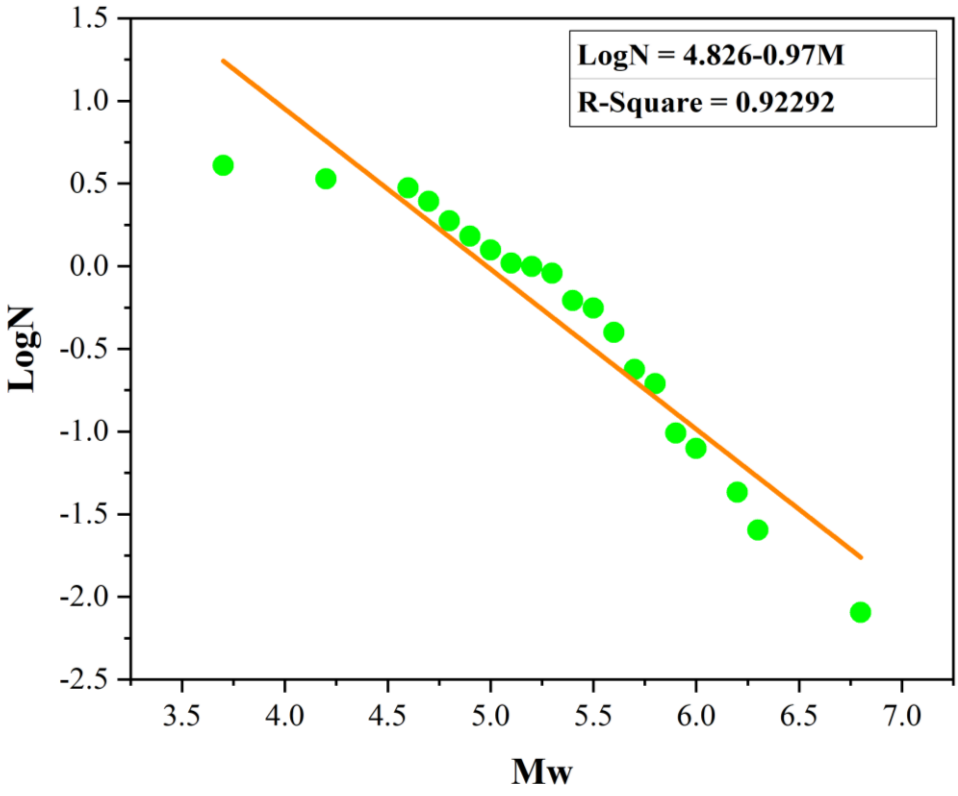

Figure 5.5: The frequency (LogN) and magnitude (Mw) relation for Kopili fault using Gumbel's method.

5.2.5. Result and discussion

Using GEV method, the b-value is 0.97, providing a more satisfactory estimate for seismic hazard parameters.

5.2.5.1. Estimation of Most probable largest earthquake magnitude

The equation of probability of non-exceedance of magnitude '*m*' (Equation 4 as mentioned in chapter 2) can be written as:

$$G(m) = e^{-66988.25e^{-2.230m}}$$

The 'H' for the region under investigation given by

$$H = \frac{\ln \alpha}{\beta} = 4.99$$

The study calculated ‘H’ as 4.99 using equation 13 (as mentioned in chapter 2). Previous research reported varied estimates: [8] found 5.5 for northeast India, [9] estimated 6.0 and 5.8 for Assam and northeast India respectively, using GEV theory, and [10] projected 5.8 for entire northeast India. For the Shillong plateau, the ‘H’ was 4.6 using GEV theory [10]. The study attributes slight deviations from existing results to differences in earthquake catalogs, source zone sizes, and observation times. Nonetheless, the study's observations align well with previous studies for the region. Figure 5.6 illustrates time vs. H(t) based on parameters listed in Table 5.2.

Table 5.2: Most probable maximum earthquake magnitude for different periods (H(t)) in the study region

Time(year)	**H(t)**	**Time(year)**	**H(t)**
1	4.982	**60**	6.818
10	6.014	**70**	6.887
20	6.325	**80**	6.947
30	6.507	**90**	6.999
40	6.636	**100**	7.047

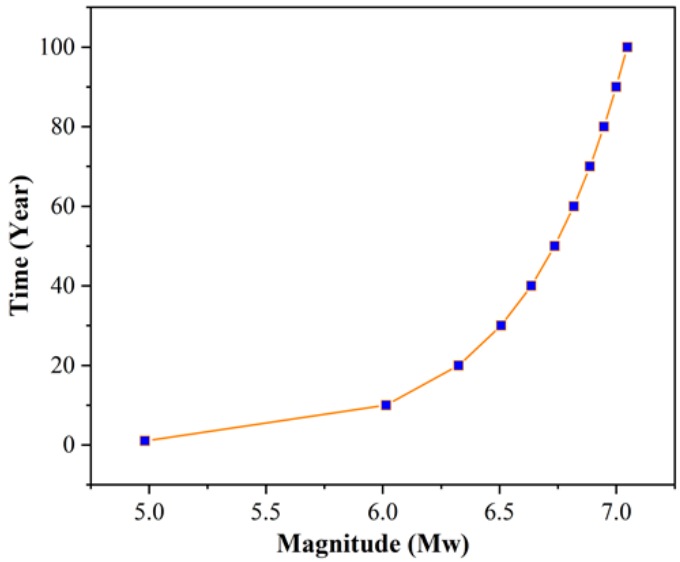

Figure 5.6: The most probable largest magnitude for a different period (H(t)).

5.2.5.2. Estimation of Return period (T(m))

Table 5.3 presents the annual expected number of earthquakes and the T(m) observed from 1964 to 2022. [10] estimated a T(m) of 23-32 years for a moderate earthquake (M_W 6.4) in the Shillong plateau region, which seems relatively high for such an active tectonic area. However, our study finds the T(m) for a M_W 6 earthquake to be approximately 10 years, which appears more realistic. The high number of annual earthquakes and short T(m) for magnitude 3.7 suggest frequent occurrences of small earthquakes over a brief period. Figure 5.7 illustrates the relationship between magnitude and T(m), showing shorter T(m) for small to medium earthquakes and longer ones for larger magnitudes.

Table 5.3: The T(m) of all the maximum magnitude earthquakes observed in the study region from 1964-2022.

Mag (M_W)	N(m)	T(m)	Mag (M_W)	N(m)	T(m)
3.7	17.484	0.057	**5.4**	0.394	2.538
4.2	5.733	0.174	**5.5**	0.315	3.174
4.6	2.350	0.425	**5.6**	0.253	3.952
4.7	1.880	0.531	**5.7**	0.202	4.950
4.8	1.504	0.664	**5.8**	0.161	6.211
4.9	1.203	0.831	**5.9**	0.130	7.692
5.0	0.962	1.039	**6.0**	0.103	9.708
5.1	0.770	1.298	**6.2**	0.066	15.151
5.2	0.616	1.623	**6.4**	0.053	18.867
5.3	0.493	2.028	**6.7**	0.017	57.803

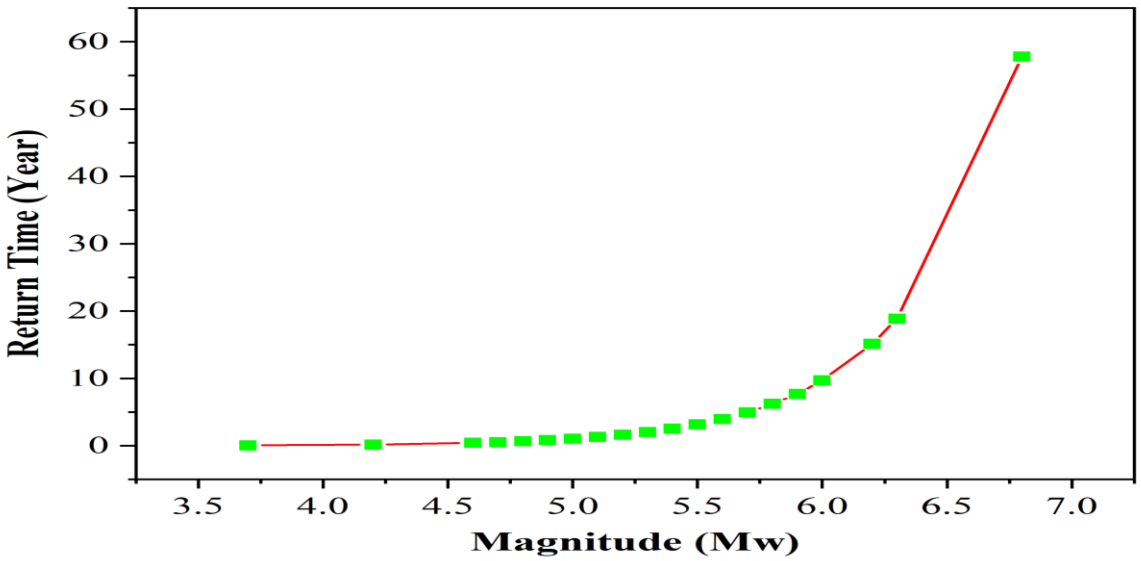

Figure 5.7: The T(m) vs magnitude curve shows the return period of maximum magnitude earthquakes observed in the region from 1964-2022.

5.2.5.3. Calculation of probability of occurrence of earthquakes with different magnitudes

The Kopili fault and its vicinity are highly seismic, with historical data pinpointing numerous significant earthquakes in this area. Utilizing Gumbel's extreme value theory, probabilities of earthquakes of varying magnitudes occurring over different periods (1, 10, 20 years, etc.) were estimated in Table 5.4. Adopting a 10-year window aimed to capture plausible seismic events, compensating for past data limitations. The probability versus magnitude curve, or hazard curve, reveals a high likelihood of small earthquakes ($M_W \leq 4.5$) within one year. Conversely, the probability of an M_W ~5 earthquake within the next decade is 95%. Extending the time frame for larger earthquakes escalates their probability, with Table 5.4 indicating an almost 99% likelihood of $M_W = 6$ earthquakes occurring within the subsequent 40 years (Figure 5.8).

Table 5.4: Probabilities of occurrence (P_t) of earthquakes for different magnitude(m) and period (t).

M(Mw)	P_1	P_{10}	P_{20}	P_{30}	P_{40}	P_{50}	P_{60}	P_{70}	P_{80}	P_{90}	P_{100}
4	0.999	1.000	1.000	1.000	1.000	1.000	1.000	1.000	1.000	1.000	1.000
4.5	0.946	1.000	1.000	1.000	1.000	1.000	1.000	1.000	1.000	1.000	1.000
5	0.617	0.999	0.999	1.000	1.000	1.000	1.000	1.000	1.000	1.000	1.000
5.5	0.270	0.957	0.998	0.999	0.999	0.999	0.999	1.000	1.000	1.000	1.000
6	0.097	0.643	0.873	0.954	0.983	0.994	0.997	0.999	0.999	0.999	0.999
6.5	0.032	0.281	0.483	0.628	0.732	0.807	0.861	0.901	0.928	0.948	0.963
7	0.010	0.104	0.197	0.281	0.355	0.423	0.483	0.536	0.585	0.628	0.667
7.5	0.002	0.029	0.058	0.086	0.113	0.139	0.164	0.189	0.213	0.236	0.259
8	0.001	0.009	0.019	0.029	0.039	0.048	0.058	0.067	0.076	0.086	0.095

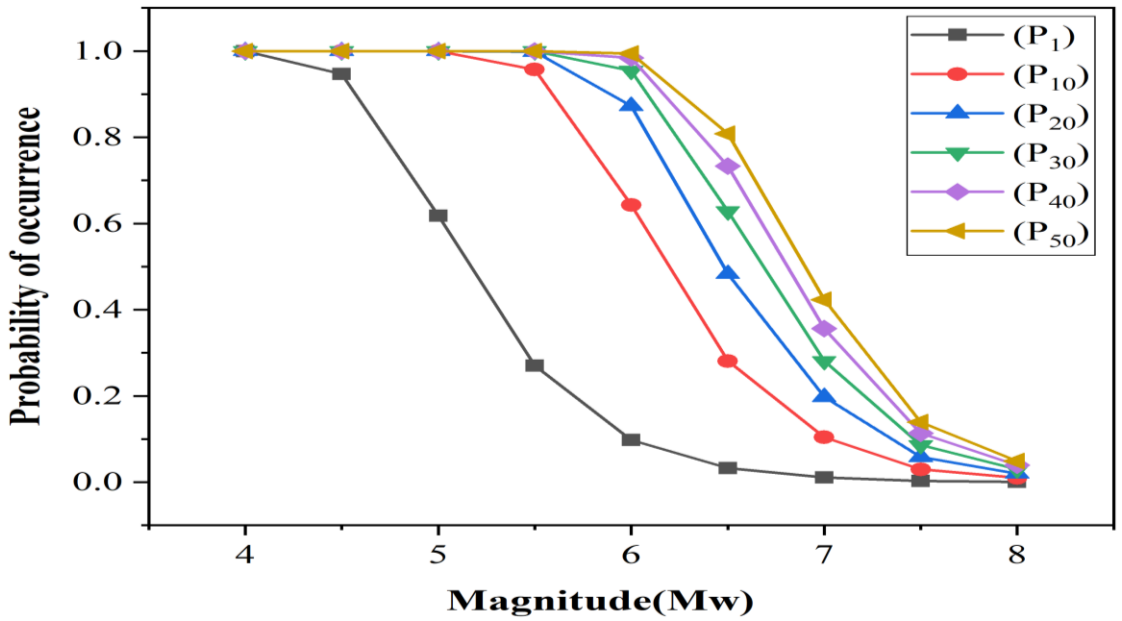

Figure 5.8: The plot showing the probability of occurrence of various magnitude at different periods.

The likelihood of large earthquakes increases with a longer time window, particularly for those with magnitudes $M_W \geq 6.5$. Over the next 100 years, the probability of a M_W 7 earthquake is 66%, while for M_W 6.5, it is 97%. However, the probability of a M_W 8 earthquake within the same timeframe is low. Small earthquakes are more probable in the short term, but the likelihood of large earthquakes increases over time. For instance, the probability of a M_W 6.5 earthquake is 80% in the next 50 years, rising to 96% over 100 years (Figure 5.9). Larger earthquakes ($M_W > 6.5$) also follow this trend. The expected maximum magnitude in the region over the next century falls between 7.0-7.5, with a probability exceeding 50%. Discrepancies in predictions with previous studies may stem from differences in earthquake catalogs over time, but these nuances are minor in probabilistic analyses.

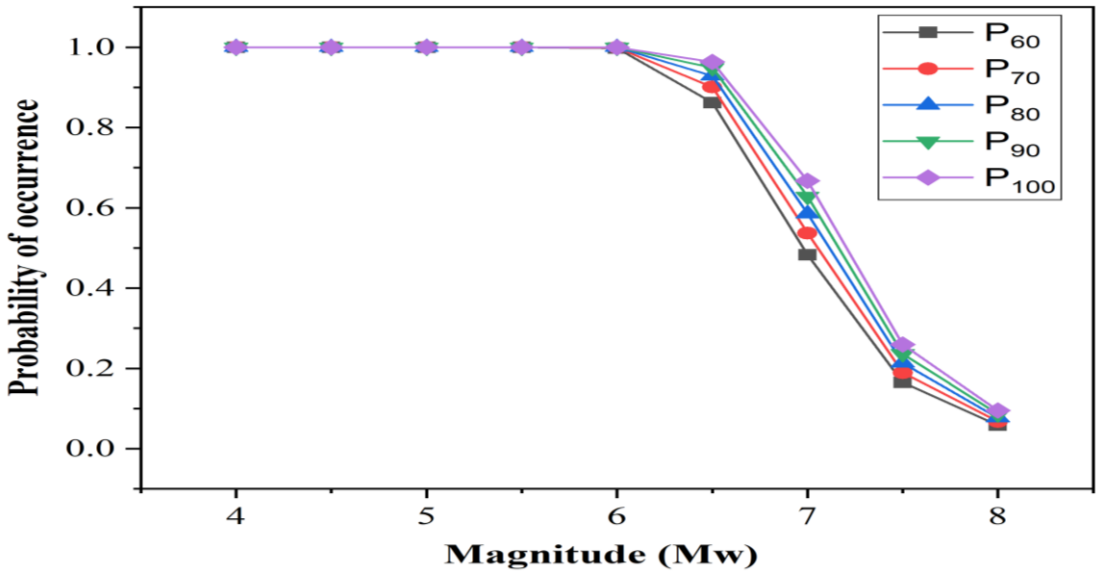

Figure 5.9: The plot shows the probability of occurrence of various magnitudes for the different periods.

5.3. Probabilistic estimation of seismic hazard attributes for Indo-Burma region of northeast India

5.3.1. Introduction

The Indo-Burma subduction zone in northeast India, known for its active tectonics, is a potential site for large earthquakes due to the Indian plate sinking beneath the Burmese plate. Researchers favor a probabilistic approach to account for all potential sources and uncertainties. This study uses statistical techniques, specifically the GEV theory ([2], [3]), to evaluate seismic hazard parameters and improve the b-value estimation. The aim is to better understand the frequency-magnitude correlation and predict the likelihood of future earthquakes in the Indo-Burma region.

5.3.2. Tectonic setup

The Indo-Burma region, encompassing the Eastern and North-eastern Himalayas, Myanmar, Bangladesh, and the Andaman-Sumatra area, features the highly active Indo-Myanmar subduction zone. This subduction zone, marked by complex deformation, involves the Indian plate subducting beneath the Burmese micro-plate in multiple directions (NE-SW, NNE-SSW, N-S). It has experienced 18 significant earthquakes (M ≥7.0) and two major earthquakes (M > 8.0) between 1897 and 2003, causing extensive damage in northeast India. The subduction process during the Cenozoic era formed the IBR. The region's seismic activity extends up to 200 km below the surface, influenced by oceanic lithosphere with a dip of 30° to 60°. The Myanmar segment of the SF, running between the Burmese lowlands and the Shan Plateau, is notably active, with the Burma earthquake of Mw ~8 being a significant event. Figure 5.10 illustrates the Seismotectonics of the IBR.

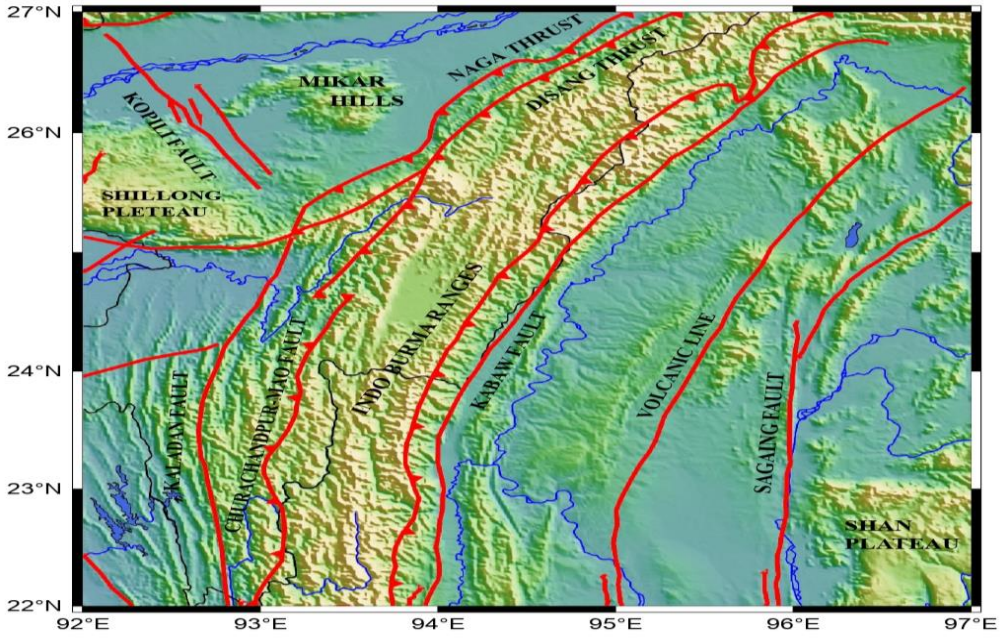

Figure 5.10: The tectonic map of the study region. Major tectonic features are marked as the kopili fault, Mikir hills, Shillong plateau, kaladana fault, CMF, KF, SF, Naga thrust, Disang thrust, and the Shan plateau.

5.3.3. Data Analysis

The study focuses on a region bounded by 22°-27°N and 92°-97°E, compiling an earthquake catalog from 1973 to 2021 sourced from the USGS and the ISC. Aftershocks and main shocks are differentiated following [11] (as mentioned in Table 2.2 of chapter 2)

method, ensuring data integrity through careful avoidance of duplication. To ensure a uniform catalog for estimating the b-value, all magnitudes are converted to M_W using conversion relations proposed by [6] and [7] (as mentioned in Table 2.1 of chapter 2).

5.3.4. Estimation of seismic hazard parameters

The Gumbel Annual Extreme Values ([2], [3]) approach are used to get the b-value for the Indo-Burma area. The regression constants after analyzing the extreme events observed from 1973 to 2021 are listed in the Table 5.5.

Table 5.5. Calculations of parameters for Gumbel's annual maximum distribution

M_W	J	f	G(m)	LnG(m)	N = -LnG(m)	$Log_{10}N$
4.8	2	0.04	0.04	-3.219	3.219	0.508
4.9	1	0.02	0.06	-2.814	2.814	0.45
5	2	0.04	0.1	-2.303	2.303	0.363
5.1	2	0.04	0.14	-1.967	1.967	0.294
5.2	1	0.02	0.16	-1.833	1.833	0.264
5.3	6	0.12	0.28	-1.273	1.273	0.105
5.4	3	0.06	0.34	-1.079	1.079	0.033
5.5	4	0.08	0.42	-0.868	0.868	-0.062
5.6	7	0.14	0.56	-0.58	0.58	-0.237
5.7	4	0.08	0.64	-0.447	0.447	-0.351
5.8	1	0.02	0.66	-0.416	0.416	-0.382
5.9	3	0.06	0.72	-0.329	0.329	-0.484
6	1	0.02	0.74	-0.302	0.302	-0.522
6.1	2	0.04	0.78	-0.249	0.249	-0.605
6.2	2	0.04	0.82	-0.199	0.199	-0.703
6.3	3	0.06	0.88	-0.128	0.128	-0.894
6.4	1	0.02	0.9	-0.106	0.106	-0.978
6.8	1	0.02	0.92	-0.084	0.084	-1.079
6.9	1	0.02	0.94	-0.062	0.062	-1.209
7	1	0.02	0.96	-0.041	0.041	-1.39
7.3	1	0.02	0.98	-0.021	0.021	-1.695

where Magnitude (M) is the magnitude of observed earthquake arranged in the increasing order, J gives the number of earthquake magnitude observed and f gives the relative frequency of earthquake calculated using formula (f=J/n+1) and G(m) gives cumulative relative frequency of the earthquake. The regression relation obtained from the Gumbel relation as shown in Figure 5.11 is given as:

$$Log_{10}N = 4.8350 - 0.902M_w \quad (9)$$

Following the least-squares technique application, as seen in Figure 5.11, the a and b values for the study area are determined to be 4.8350 and 0.902, respectively. Thus, the Gumbel's coefficient α and β after using a and b-value are found to be α = 68391.16 and β = 2.08 respectively.

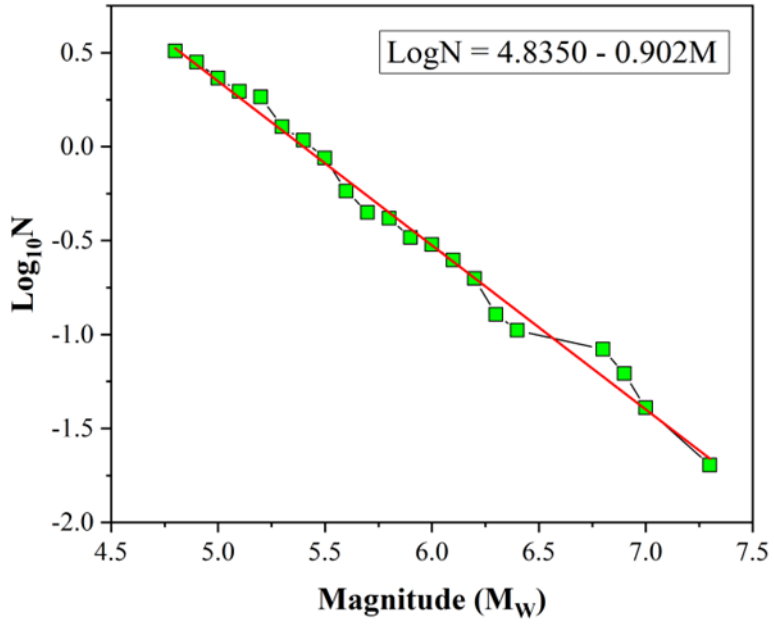

Figure 5.11: The relation between frequency (Log10N) and magnitude (Mw) observed using Gumbel's method for the Indo-Burma region.

5.3.5. Result and Discussion

5.3.5.1. Estimation of Most probable largest earthquake magnitude

The Gumbel parameters derived from a and b-values are used to estimate the 'H' for the study area. As per present analysis, the 'H' of 5.352 is found for the Indo-Burma region. Previous studies by [8] suggested 5.5, while [9] found values of 6.0 for Assam and 5.8 for northeast India using GEV theory. [10] reported an 'H' of 5.8 for northeast India and 5.5

for the Arakan-Yoma subduction zone within the Indo-Burma region. This aligns closely with our findings, affirming consistency across research in the area. Furthermore, the estimation of H(t) for earthquakes over time period (t) is also computed. Detailed results are provided in Table 5.6, including the H(t) expected within the next hundred years (as shown in Figure 5.12).

Table 5.6: Most probable maximum earthquake magnitude for different periods (H(t)) in the study region

Time(year)	H(t)
1	5.352
10	6.459
20	6.792
30	6.987
40	7.125
50	7.232
60	7.320
70	7.394
80	7.458
90	7.515
100	7.566

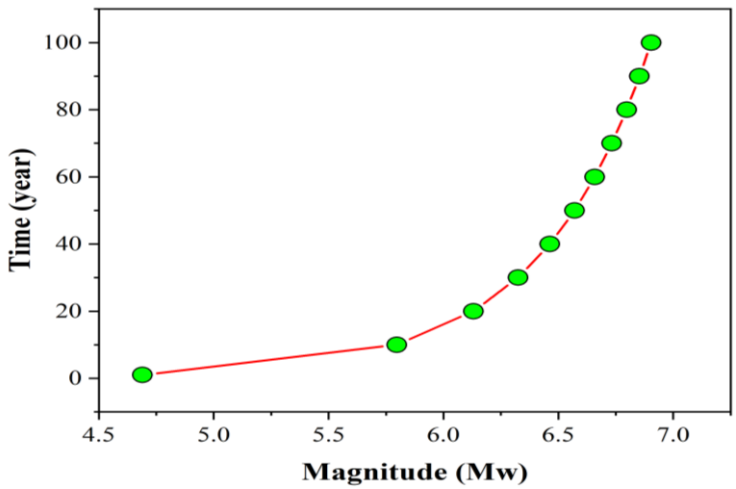

Figure 5.12: The most probable largest magnitude for a different period

5.3.5.2. Estimation of Return period (T(m))

The T(m) for earthquakes of magnitude (m) is calculated as the inverse of N(m), the number of earthquakes with magnitudes equal to or greater than (m) recorded annually. Table 5.7 provides the annual forecasted earthquake numbers and T(m) observed from 1973 to 2021. Figure 5.13 illustrates the relationship between return time and magnitude, showing shorter return times for small to medium-sized earthquakes and longer periods for major earthquakes.

Table 5.7: The T(m) of all the maximum magnitude earthquakes observed in the study region from 1973-2021.

Magnitude (M_W)	Time (year)	N (m)
4.8	0.317	3.156
4.9	0.391	2.563
5.0	0.481	2.082
5.1	0.592	1.691
5.2	0.729	1.374
5.3	0.897	1.116
5.4	1.105	0.906
5.5	1.36	0.736
5.6	1.674	0.598
5.7	2.061	0.486
5.8	2.538	0.395
5.9	3.124	0.321
6.0	3.846	0.261
6.1	4.736	0.212
6.2	5.83	0.172
6.3	7.178	0.14
6.4	8.838	0.114
6.8	20.308	0.05
6.9	25.004	0.04
7.0	30.785	0.033
7.3	57.455	0.018

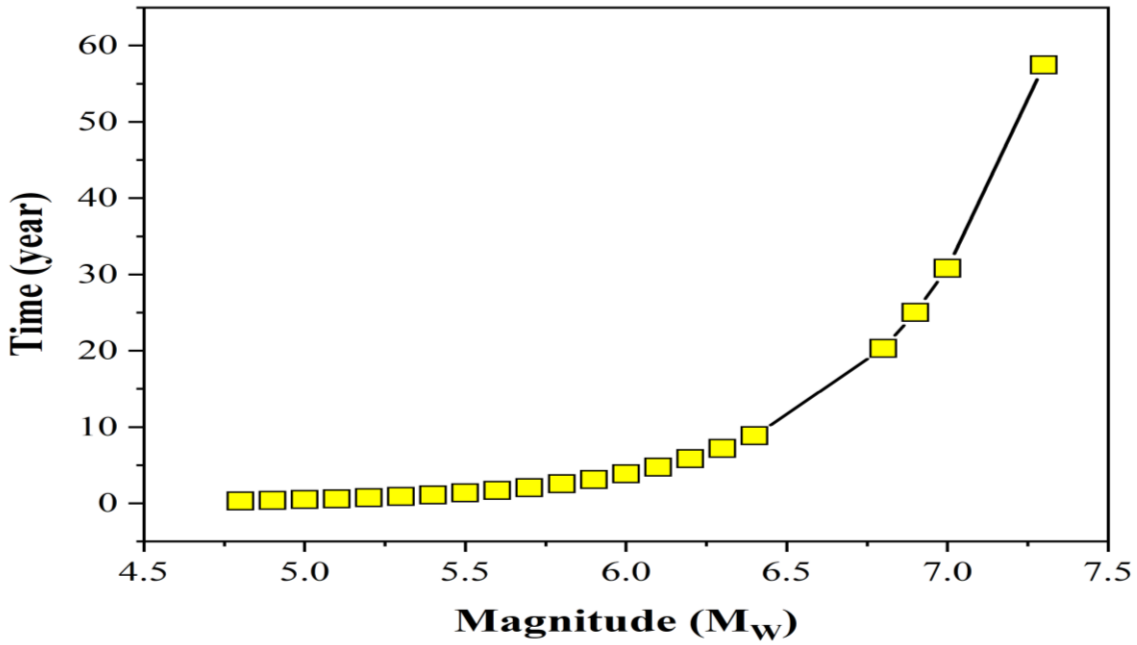

Figure 5.13: The T(m) vs magnitude curve shows the return period maximum magnitude earthquakes observed in the region from 1973-2021.

5.3.5.3. Calculation of probability of occurrence of earthquakes with different magnitudes (P(t))

Historical data revealed that the epicenter of several significant earthquakes is traceable in the Indo-Burma area, which is one of the seismically active regions of NE India and the world. The likelihood of various magnitude earthquakes occurring over different periods (1,10,20...) with a time interval of 10 years has been estimated using GEV theory, and the results are shown in Table 5.8 and Figure 5.14. The key rationale for choosing a 10-year window is because it has become more difficult to anticipate earthquakes over a long period of time owing to rapid changes in the earth's crust and the ability to identify practically every seismic event that happens in an area thanks to advances in seismic hazard research. The hazard curve, also known as the probability of occurrence vs. magnitude curve, indicates the likelihood that the corresponding magnitude will occur. It is clear from Table 5.8 and Figure 5.14 that there is a good chance that minor earthquakes with a magnitude of Mw ≤ 5 will occur within a year. On the other hand, if we looked at the likelihood of a Mw 5.5 earthquake happening in the next 10 years, the chance is 100%. Similar to this, the likelihood of major earthquakes occurring rises as we extend the time span.

Table 5.8: Probabilities of occurrence (P_t) of earthquakes for different magnitude(m) and period (t)

M_W	P_1	P_{10}	P_{20}	P_{30}	P_{40}	P_{50}	P_{60}	P_{70}	P_{80}	P_{90}	P_{100}
4	1	1	1	1	1	1	1	1	1	1	1
4.5	0.998	1	1	1	1	1	1	1	1	1	1
5	0.876	1	1	1	1	1	1	1	1	1	1
5.5	0.521	1	1	1	1	1	1	1	1	1	1
6	0.23	0.927	0.995	1	1	1	1	1	1	1	1
6.5	0.088	0.602	0.842	0.937	0.975	0.99	0.996	0.999	1	1	1
7	0.033	0.282	0.484	0.629	0.733	0.808	0.862	0.901	0.929	0.949	0.964
7.5	0.012	0.114	0.214	0.303	0.382	0.452	0.514	0.569	0.618	0.661	0.699
8	0.005	0.049	0.096	0.14	0.182	0.222	0.26	0.296	0.33	0.363	0.394

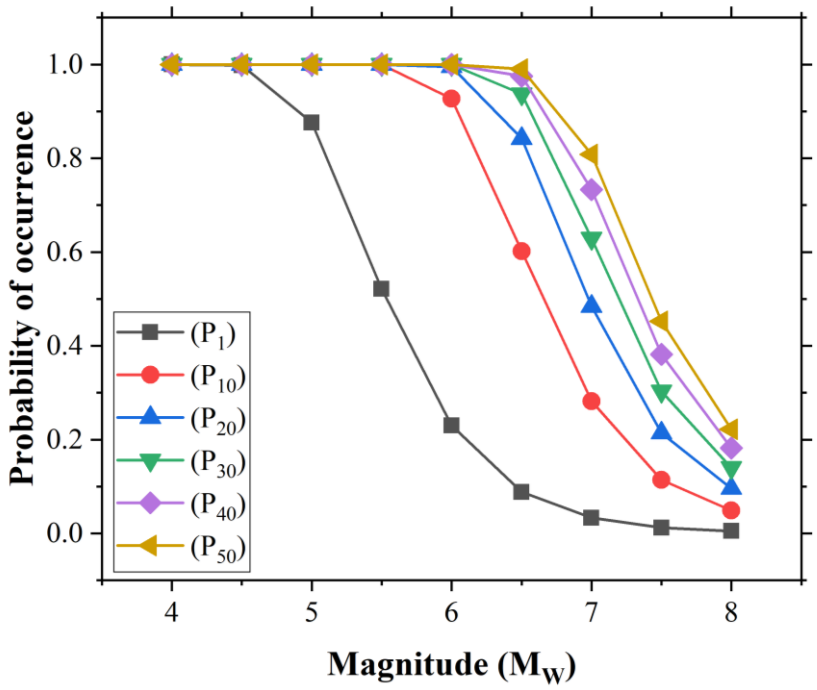

Figure 5.14: The plot shows the probability of occurrence of various magnitude at different periods.

Now, when we extend the time frame even more, there is a higher chance that major earthquakes may occur. As the time frame is extended, the likelihood of an earthquake with a magnitude of Mw ≥ 6.5 grows. The likelihood of an earthquake of magnitude Mw 7

occurring in the next 100 years is determined to be 96%, whereas the probability of an earthquake of magnitude Mw 6.5 occurring in that time is found to be 100%. The likelihood of an earthquake of Mw8 magnitude occurring is quite low, and we can assume that we will seldom ever see an earthquake of Mw8 in this area in the next 100 years. Now, if we split the earthquakes according to their magnitudes, we can see that the likelihood of tiny earthquakes occurring is fairly high. Additionally, the table shows that a lot of small to medium earthquakes may happen in the following years. However, the likelihood of major earthquakes happening grows with time. For example, the likelihood of an earthquake of magnitude Mw 6.5 occurring in the next 50 years is 99%, but the likelihood climbs to 100% in the next 100 years (Figure 5.15). Similar findings may be drawn for big earthquakes with Mw > 6.5. As such occurrences are more likely to occur than 50% of the time, the largest magnitude that may be detected in this area in the next 100 years will be between 7 and 7.5. Similar implications were made by [10] the modest differences between our observations and previous studies could be related to the separate earthquake catalog created for various time periods, there may be a little discrepancy between our findings and the research that have already been done. But such small differences in observations can be ignored in probabilistic approaches. As a result, we can state that our study's findings are consistent with recent research in the area.

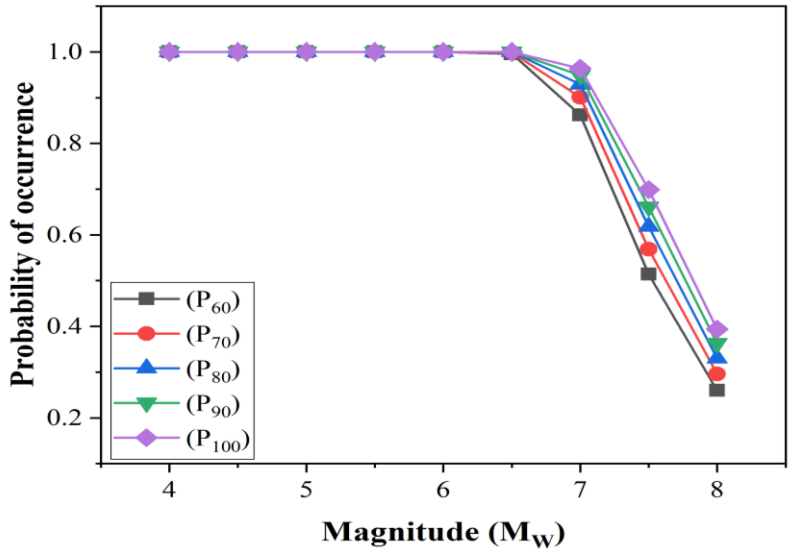

Figure 5.15: The plot shows the probability of occurrence of various magnitudes for the different periods.

5.4. Probabilistic estimation of seismic hazard attributes for East Anatolian Fault Zone (EAFZ) of Türkiye

5.4.1. Introduction

Türkiye form a complex tectonic setting, where four major plates converge, drives various geological processes including earthquakes and volcanic activity [12]. Seismicity is prominent, especially along the Aegean Arc due to African and Eurasian plate convergence, and the NAFZ facilitates westward movement of the Anatolian Plate. In the east, the EAFZ, spanning 700 km, marks the Anatolian-Arabian plate boundary, renowned for major earthquakes [13]. The recent Kahramanmaraş earthquake doublet (M_W 7.8; M_W 7.6) on February 6, 2023, occurred along the EAFZ. The epicentral location of the major events observed in this region is illustrated in the Figure 5.16 and listed in Table 5.9.

Table 5.9: The focal parameters of the large (M > 6.0) earthquakes occurred in the study area spanning from 1882 to 2020.

S.no	Date (d/m/y)	Longitude (^{0})	Latitude (^{0})	Magnitude
1	13/08/1822	39.90	36.70	7.5 M_S
2	12/05/1866	41.00	39.20	7.2 M_S
3	03/04/1872	36.50	36.40	7.2 M_S
4	03/05/1874	39.50	38.50	7.1 M_S
5	27/03/1875	39.50	38.50	6.7 M_S
6	02/03/1893	38.30	38.00	7.1 M_S
7	04/12/1905	38.60	38.10	6.8 M_S
8	07/05/1930	44.70	38.10	7.5 M_S
9	19/08/1966	41.56	39.17	6.8 Mw
10	22/05/1971	40.52	38.83	6.9 Mw
11	06/09/1975	40.70	38.50	6.6 M_S
12	13/03/1992	39.69	39.70	6.7 Mw
13	27/06/1998	35.31	36.88	6.3 Mw
14	27/01/2003	39.79	39.46	6.1 Mw
15	01/05/2003	40.46	39.01	6.4 Mw
16	08/03/2010	40.03	38.79	6.1 Mw
17	23/10/2011	43.49	38.63	7.2 Mw
18	24/01/2020	39.08	38.39	6.8 Mw

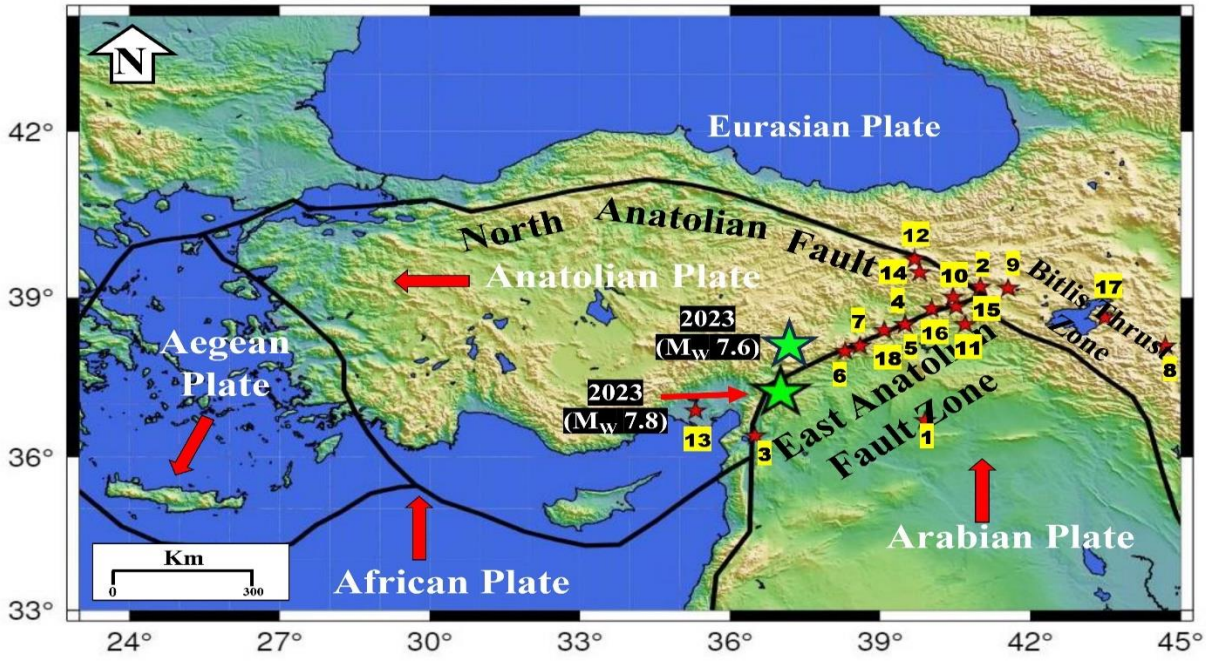

Figure 5.16: The geographic plate boundaries surrounding Türkiye including the Anatolian Plate, Eurasian Plate, Arabian Plate, African Plate, and Aegean Plate highlighting the complex geologic setting of the region. The epicenters of 6th February 2023 Kahramanmaraş earthquake (M_W 7.8) and the Elbistan earthquake (M_W 7.6) are shown by green star. The epicenter of major earthquakes ($M \geq 6.1$) observed along the EAFZ is shown by red star.

In this study, we segment the EAFZ into fault sections, including the Amanos, Pazarcık, Erkenek, Pütürge, Palu, Karlıova, and Çardak fault sections, following [14]. While seismic parameters have been estimated for Türkiye and the EAFZ, few studies focus on individual fault segments. [15] linked the February 6, 2023 Kahramanmaraş earthquake doublet (M_W 7.8, M_W 7.6) to the Amanos, Pazarcık, Erkenek, and Çardak fault sections. We estimate seismic parameters like the a and b-values, maximum annual earthquake, return period, and earthquake magnitude likelihood for these fault sections using the GEV approach ([2], [3]).

5.4.2. Tectonic setup

In eastern Türkiye, the EAFZ is a significant tectonic feature formed by interactions among the Anatolian, Eurasian, and Arabian Plates [16]. The Anatolian Plate moves

westward at about 24 ± 2 mm/year, while the Arabian Plate moves northward at approximately 15 ± 2 mm/year [17], contributing to increased seismic activity (as shown in Figure 5.17). The EAFZ, initially identified by [18] and mapped by [19], spans about 700 kilometers from the Karlıova Triple Junction (KTJ) in the north to Antakya near the Dead Sea Fault Zone (DSFZ) in the south [20]. The Varto Fault Zone (VFZ), southeast of KTJ, exhibits right-lateral strike-slip motion. The Kahramanmaraş Triple Junction marks a convergence point for the EAFZ, DSFZ, and Karataş-Osmaniye Fault [16]. Another DSFZ segment terminates at the Amanos Fault, while the Antakya Graben lies between the Amik Basin and the Mediterranean Sea, shaping EAFZ activity. In the north, compression between the Eurasian and Anatolian Plates drives westward movement, while to the south, convergence with the Arabian Plate results in subduction beneath the Anatolian Plate.

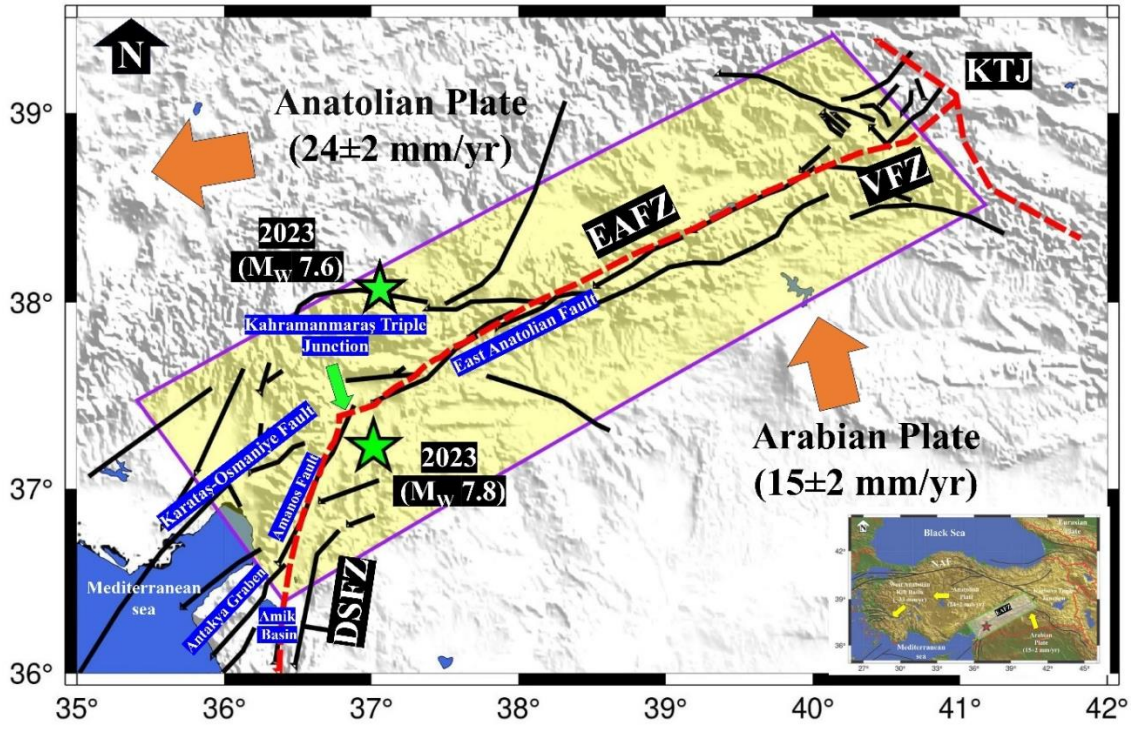

Figure 5.17: The seismotectonic map of the Eastern-Türkiye consisting of major active structure namely: EAFZ; DSFZ; KTJ; and VFZ; the Kahramanmaraş Triple Junction; the Karataş-Osmaniye Fault; the Amanos Fault; the Antakya Graben; the Amik Basin. The study area is highlighted by yellow color. The plate boundary between the Anatolian plate, the Eurasian plate and the Arabian plate is illustrated by the red dashed line. The relative rate of motion of Arabian plate and the Anatolian fault is also mentioned with the orange arrow. The epicenters of 6th February 2023 Kahramanmaraş earthquake doublet (M_W 7.8, M_W 7.6) are shown by green star. The inset map of Türkiye is also attached in the figure.

The EAFZ has seen seven major earthquakes (M > 6.0) since the twentieth century, creating two seismic gaps [14]. One gap, linked to the Pütürge fault section, was ruptured by the 2020 Mw 6.8 Sivrice earthquake [15]. The other gap is in the Pazarcık fault section, noted for its potential to trigger destructive earthquakes of Mw ≥ 7.3 [15]. The EAFZ trends northeastward between Pazarcık and Palu, shifting to north-northeastward at Amanos. Slip rates decline along the fault, dropping further along the Amanos section [15]. Despite central and northern segments being the most active, seismic strain decreases southwestward, transferring to subsidiary faults like Çardak [15]. Consequently, the southwestern part of the EAFZ, including Amanos, Pazarcık, Erkenek, and Çardak sections, could generate large earthquakes despite long-term low slip rates (as shown in Figure 5.18). The Kahramanmaraş earthquake doublet on February 6th, 2023 (M_W 7.8, M_W 7.6), addressed a seismic gap on the Pazarcık fault section. The EAFZ, known for producing moderate to large earthquakes, poses a significant seismic risk due to accumulated stress from tectonic motions, making it one of the most active seismic regions in Türkiye.

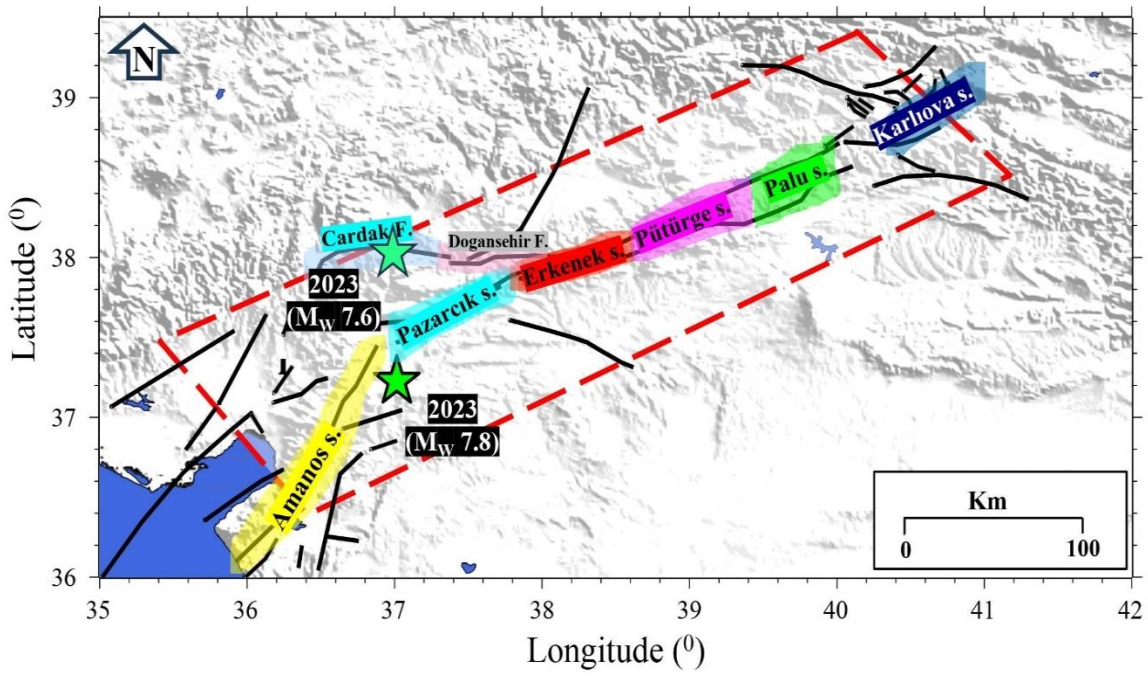

Figure 5.18: Segmentation of the EAFZ, utilizing color-coded bands to denote distinct fault sections, as delineated by [14].

5.4.3. Data Analysis

A unified earthquake catalog from 1905 to October 2018, covering magnitudes M_W 2.5 to M_W 6.9, was compiled from [13]. Data from KOERI, ISC, and USGS databases from November 1, 2018, to January 31, 2023, were also added. Magnitudes (M_D, M_S, M_L, mb, M, M_W) were standardized to M_W using conversion method proposed by [13] (as mentioned in Table 2.1 of chapter 2). Declustering to separate dependent events (foreshocks and aftershocks) is performed using the method proposed by [21] (as mentioned in Table 2.3 of chapter 2). The Zmap tool assisted in this process, identifying 8,453 background earthquakes for further analysis after removing 698 dependent events.

The cumulative distribution of these independent events is illustrated in the accompanying Figure 5.19.

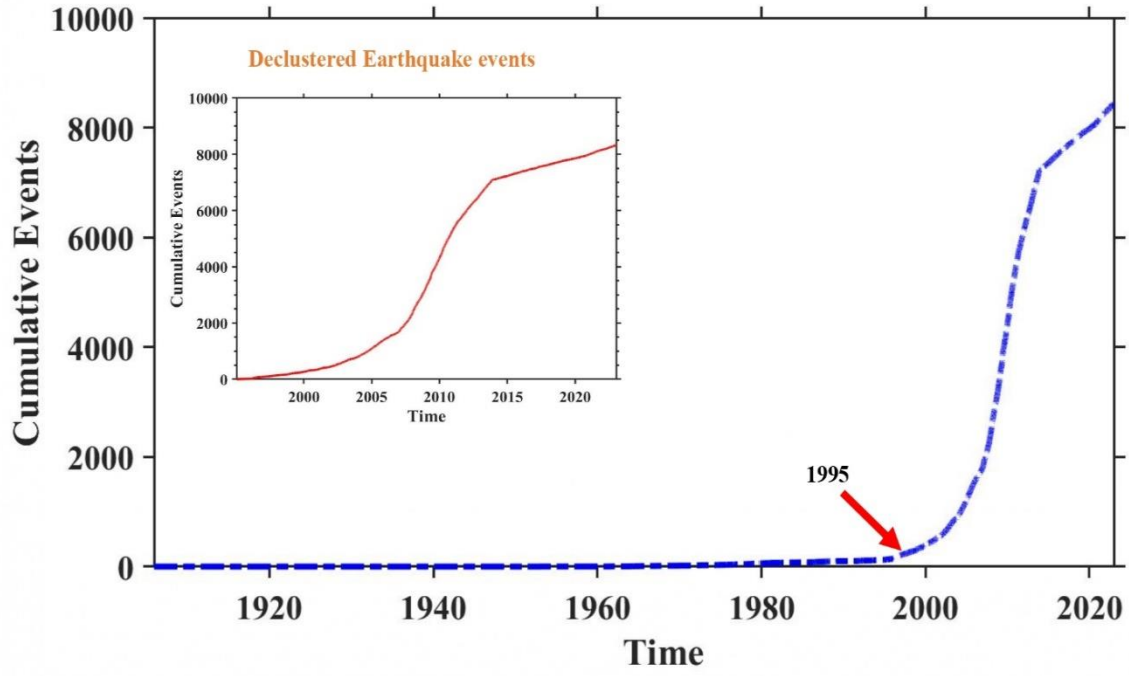

Figure 5.19: The cumulative number of events vs time plot for the declustered earthquake catalog.

After declustering, the temporal completeness period of the earthquake catalog was established using the CUVI method from [22]. By examining the cumulative number of events over time (Figure 5.20), the completeness period was identified as 1995 to 2023. The M_C was calculated using the MAXC method by [23], with a correction factor of '+0.2' for accuracy as suggested by [24]. The FMD curves obtained are shown in Figure 5.20.

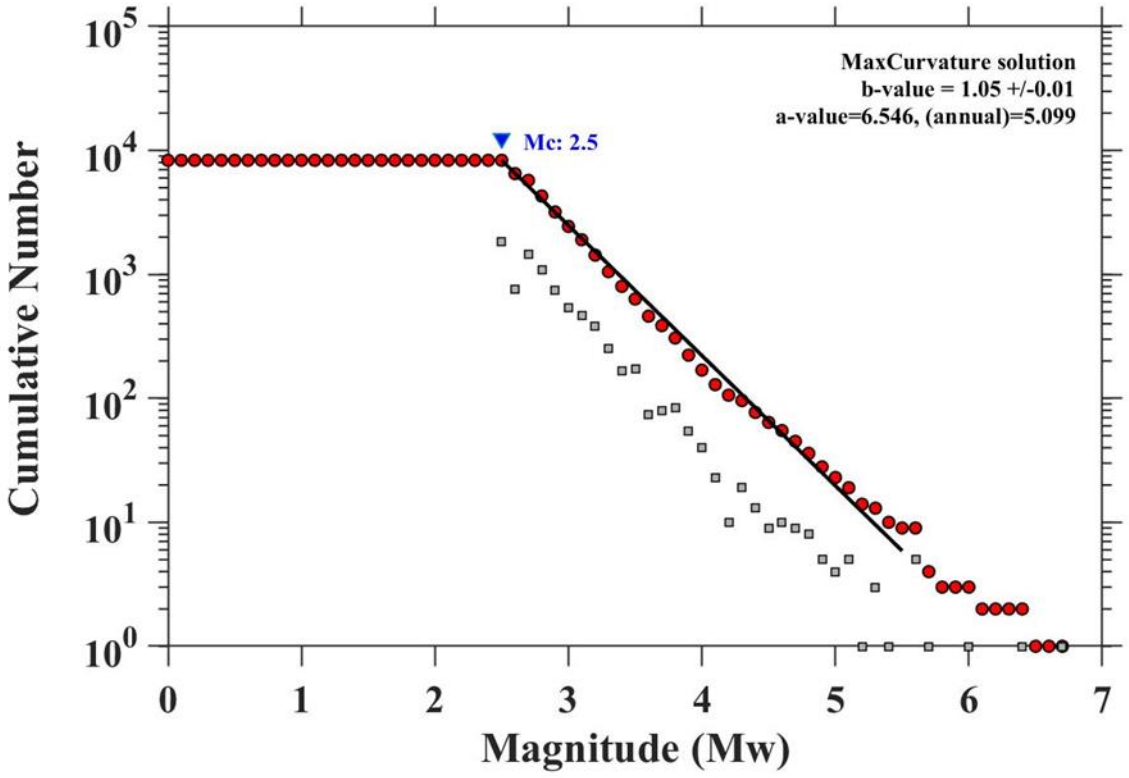

Figure 5.20: The FMD curve obtained using the MAXC approach for the earthquake catalog scaled at M_W scale.

The earthquake catalog analysis focused on events with magnitudes $M_W \geq 2.5$, selecting an M_C of 2.5. Temporal changes in M_C were analyzed using a sliding window technique and bootstrapping, revealing a range from 4.7 to 2.5. Higher M_C values (4.7 to 3.6) were observed from 1905 to 1994, decreasing from 1995 to 2023, reflecting increased seismic activity due to improved detection capabilities (as shown in Figure 5.21). The M_C value is influenced by the number of recorded events, decreasing over time as more seismic stations enable detection of minor events, consistent with [25] findings on M_C variations in the EAFZ.

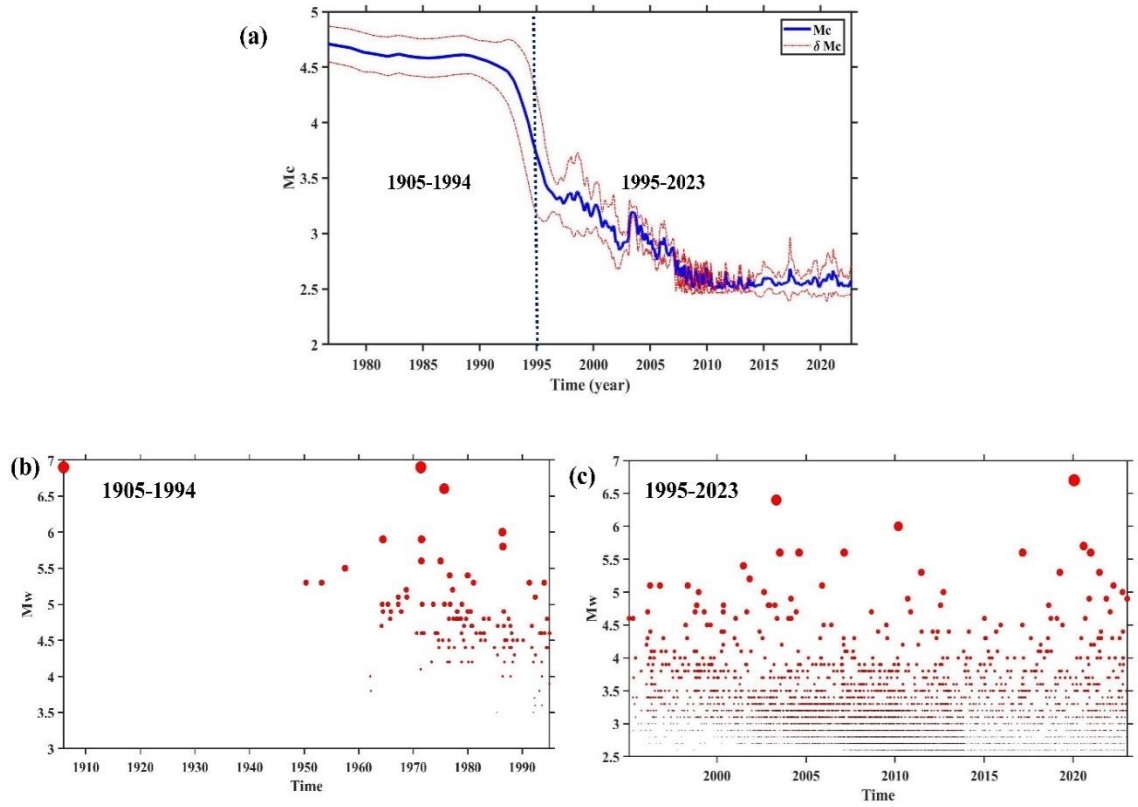

Figure 5.21: The plot illustrates the (a) temporal vartion of M_C for the period 1905 to 2023 (b) the temporal distribution of earthquakes for period 1905 to 1994 and (c) for the period 1995 to 2023.

The spatial distribution of M_C values (Figure 5.22) shows higher values from 1905 to 1994, decreasing from 1995 to 2023. This fluctuation is due to variations in the number of recorded events. The earthquake catalog is complete for $M_W \geq 2.5$ for the period 1995 to 2023 (Figure 5.22).

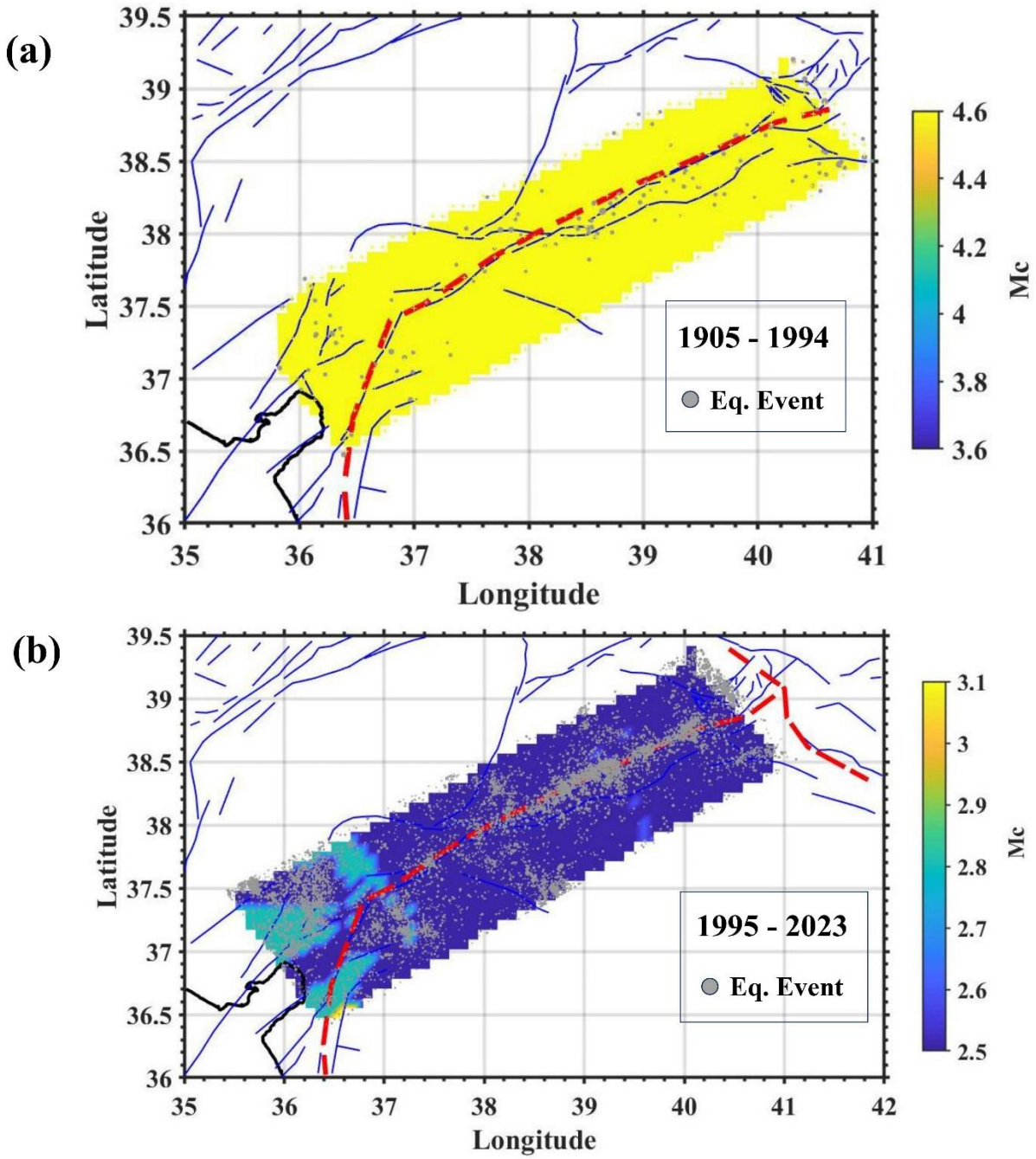

Figure 5.22: The spatial distribution of M_C value for the period (a) 1905-1994 and (b) 1995-2023 in the study region.

The M_C value for the entire study region is 2.5, indicating completeness for events with magnitudes M_W 2.5 to M_W 6.9. Epicentral locations of these events are shown in Figure 5.23.

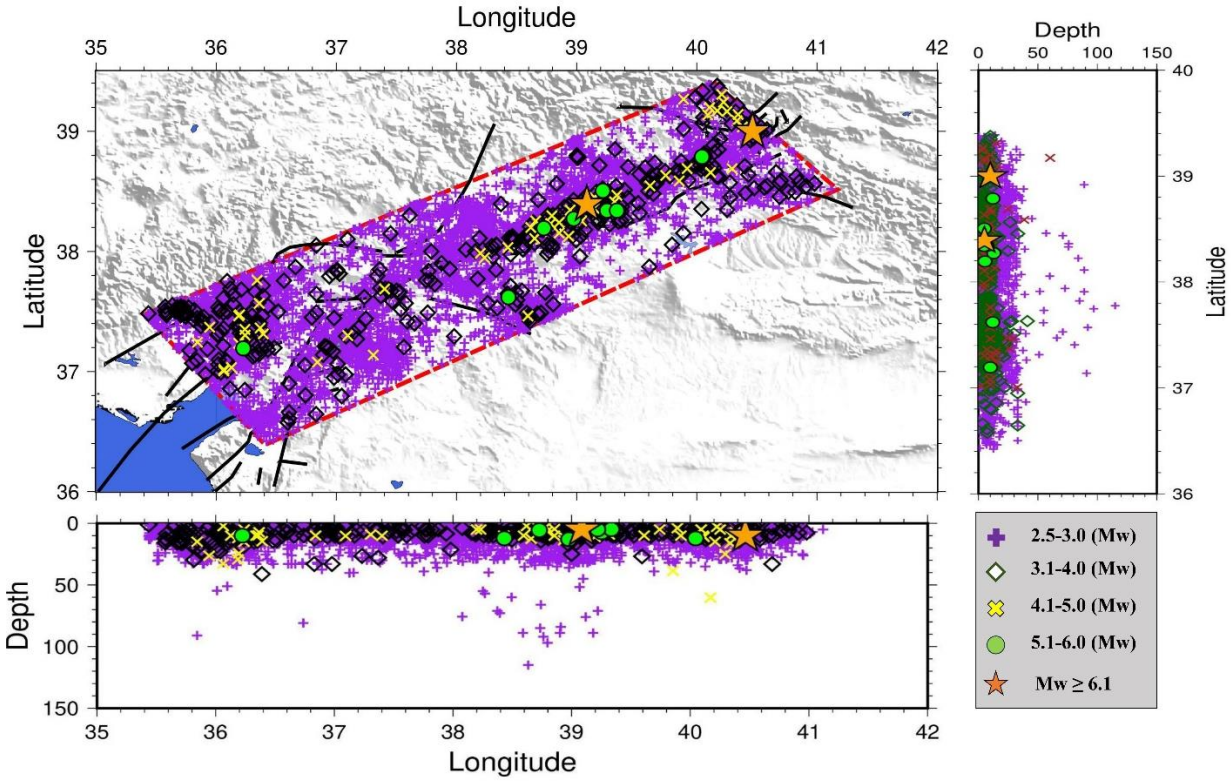

Figure 5.23: The epicentral locations of declustered, consistent earthquakes ($M_W \geq 2.5$) in the study area, along with the EAFZ and depth distribution, are shown in the figure.

5.3.4. Estimation of seismic hazard parameters

The EAFZ is a highly seismically active region, comprising segments like the Amanos, Pazarcık, Erkenek, Pütürge, Palu, Karlıova, and Çardak fault sections (Figure 5.18) [14]. Recent studies indicated the epicenter of the February 6, 2023 earthquake (M_W 7.8) near the Amanos and Pazarcık sections, while the second event (M_W 7.6) was near the Çardak section [15]. This study focuses on the seismic characterization of the Amanos, Pazarcık, Erkenek, and Çardak sections, estimating the H(t), T(m), and P(t). The GEV approach ([2], [3]) was used for seismic hazard evaluation. Figure 5.24 shows the FMD curves for these sections, and Table 5.10 lists the a, b, and M_C values obtained.

Table 5.10: The a, b and the M_C observed for the three fault sections.

S.No.	Fault Section	a-value	b-value	M_C
1	Amanos fault section	5.947	1.04 ± 0.02	2.5
2	Pazarcık fault section	6.001	1.18 ± 0.03	2.5
3	Erkenek fault section	6.720	1.55 ± 0.06	2.5
4	Çardak fault section	5.120	1.27 ± 0.18	2.6

The Erkenek fault section shows the highest a-value and b-value, indicating lower stress levels due to frequent small earthquakes. The Amanos fault section has the lowest b-value, suggesting high stress accumulation, which contributed to the February 6, 2023, Kahramanmaraş earthquake doublet (M_W 7.8; M_W 7.6). The M_C values for all four fault sections are identical. The observed a-values (2.0 to 8.0) ([26], [27]) and b-values (0.5 to 1.5) align with previous studies [28]. Smaller b-values correlate with frequent large earthquakes, while larger b-values indicate frequent small earthquakes. The Amanos section has a higher potential for large earthquakes (as shown in Table 5.10). Historical data show similar b-values for the DSFZ and parts of the EAFZ, with slight deviations due to study area, segmentation methods, and catalog periods.

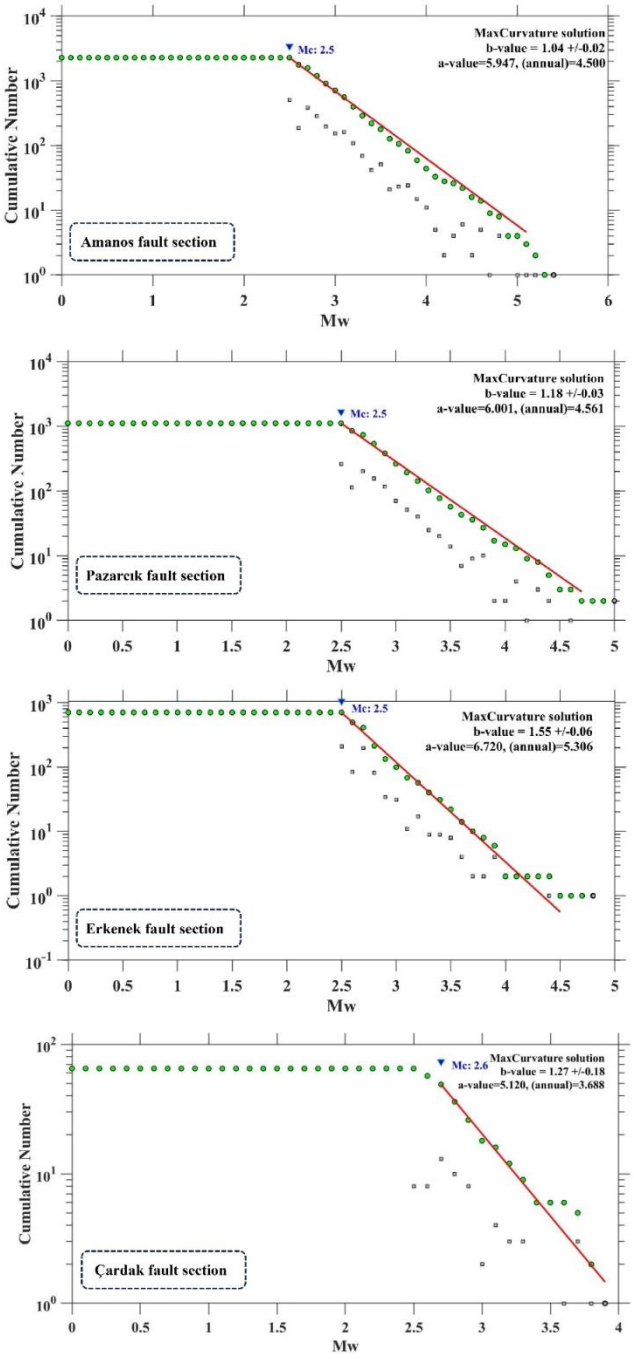

Figure 5.24: The FMD curves for the Amanos fault section, the Pazarcık fault section, the Erkenek fault section and the Çardak fault section are shown in the figure.

5.4.5. Results and Discussion

5.4.5.1. Estimation of Most probable largest earthquake magnitude

The maximum likelihood annual earthquake (H) for these fault sections, calculated using Equation 12 (as mentioned in chapter 2) are listed in Table 5.11. The highest H value is recorded for the Amanos fault section.

Table 5.11: The Peak anticipated annual earthquakes (H) along these fault sections are listed.

S.No.	Fault Section	α	β	H
1	Amanos fault section	885115.6	2.4	5.7 (Mw)
2	Pazarcık fault section	1002305	2.72	5.1 (Mw)
3	Erkenek fault section	5248075	3.57	4.3 (Mw)
4	Çardak fault section	131825.7	2.9	4.1 (M_W)

The maximum likelihood earthquake magnitudes (H(t)) for periods ranging from 1 to 100 years are estimated using Equation 13 (as mentioned in chapter 2) and listed in Table 5.12.

Table 5.12: The maximum probable magnitude (H(t)) for the period of 100 years are listed.

Time (Years)	H(t)	H(t)	H(t)	H(t)
	Amanos Fault section	Pazarcık fault section	Erkenek fault section	Çardak fault section
	M_W	M_W	M_W	M_W
1	5.70	5.10	4.30	4.10
10	6.66	5.95	4.94	4.89
20	6.95	6.2	5.14	5.13
30	7.12	6.35	5.25	5.27
40	7.24	6.46	5.33	5.37
50	7.33	6.54	5.4	5.45
60	7.41	6.61	5.45	5.51
70	7.47	6.66	5.49	5.56
80	7.53	6.71	5.53	5.61
90	7.57	6.75	5.56	5.65
100	7.62	6.79	5.59	5.69

Figure 5.25 shows that H(t) values over the next 100 years are higher for the Amanos fault section compared to the Pazarcık, Erkenek, and Çardak fault sections.

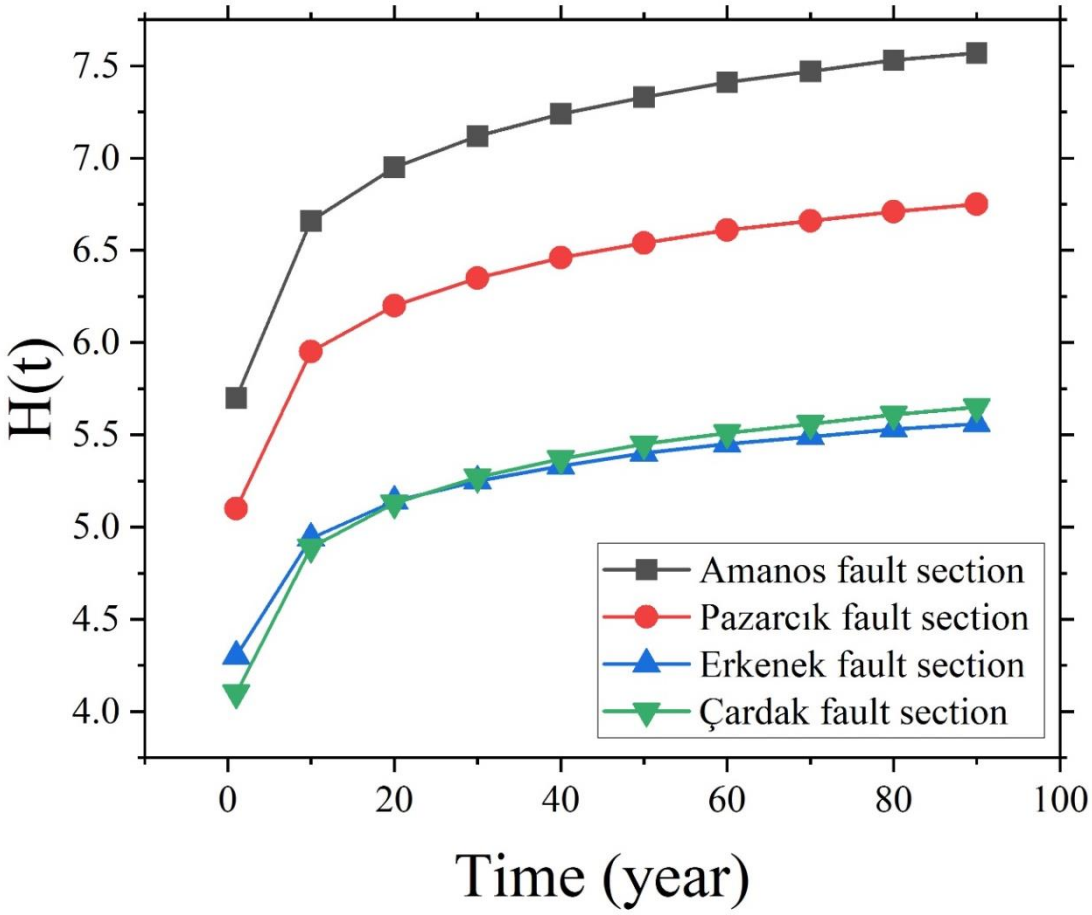

Figure 5.25: The H(t) versus time plot of the study region.

5.4.5.2. Estimation of Return period (T(m))

Equation 14 (as mentioned in chapter 2) estimates T(m) for different magnitudes, with values listed in Table 5.13. T(m) increases exponentially for larger earthquakes. Study by [14] identified the Amanos fault section as the source of the 1822 Aleppo earthquake (M 7.5). Table 5.13 suggests a magnitude M_W 7.5 earthquake occurs approximately every 180 years along this fault section, aligning with the lack of such events in the past 180 years. [15] linked the 2023 Kahramanmaraş earthquake (M_W 7.8) to the Amanos fault section, estimating a 355-year return period. Return periods are significantly longer for the Pazarcık, Erkenek, and Çardak fault sections, indicating less frequent major earthquakes.

Table 5.13: The T(m) in years for different magnitudes are listed.

Magnitude	Amanos fault section	Pazarcık fault section	Erkenek fault section	Çardak fault section
Mw	**T(Mw)**	**T(Mw)**	**T(Mw)**	**T(Mw)**
2.5	0.0005	0.0009	0.0014	0.0107
3.0	0.0015	0.0035	0.0085	0.0455
3.5	0.0050	0.0136	0.0509	0.1941
4.0	0.0167	0.053	0.3032	0.8276
4.5	0.0554	0.2064	1.8069	3.5281
5.0	0.1839	0.8043	10.7685	15.0408
5.5	0.6105	3.1336	64.1759	64.1205
6.0	2.0269	12.2092	-	-
6.5	6.7297	47.5693	-	-
7.0	22.3433	185.3391	-	-
7.5	74.1824	-	-	-

5.4.5.3. Computation of probability of occurrence of earthquakes with different magnitudes

Using Equation 15 (as mentioned in chapter 2), we calculate earthquake probabilities for various magnitudes (M_W) over ten, fifty, and one hundred years. Table 5.14 lists these probabilities, and Figure 5.26 illustrates them for the Amanos fault section. The Figure 5.26 shows a 100% probability of earthquakes with magnitudes 2.5 to 6.0 within fifty years and over 50% probability for $M_W \geq 6.5$. [29] found a 0.96 probability for an M_S 5.0 earthquake in the Kırıkhan-Islahiye section over the next hundred years. Similarly, our study shows a 1.0 probability for an M_W 5.0 earthquake in the Amanos fault section over the same period.

Table 5.14: The likelihood of occurrence of different earthquakes scaled at M_W scale for next 10, 50 and 100 years for the Amanos fault section.

Magnitude	Amanos fault section		
M_W	**P_{10}**	**P_{50}**	**P_{100}**
2.5	1	1	1
3.0	1	1	1
3.5	1	1	1
4.0	1	1	1
4.5	1	1	1
5.0	1	1	1
5.5	1	1	1
6.0	0.9928	1	1
6.5	0.77371	0.99941	1
7.0	0.36082	0.89331	0.98862
7.5	0.12611	0.49034	0.74025

Furthermore, the probabilities of occurrence for different earthquake magnitudes (M_W) for the Amanos fault section is illustrated in Figure 5.26.

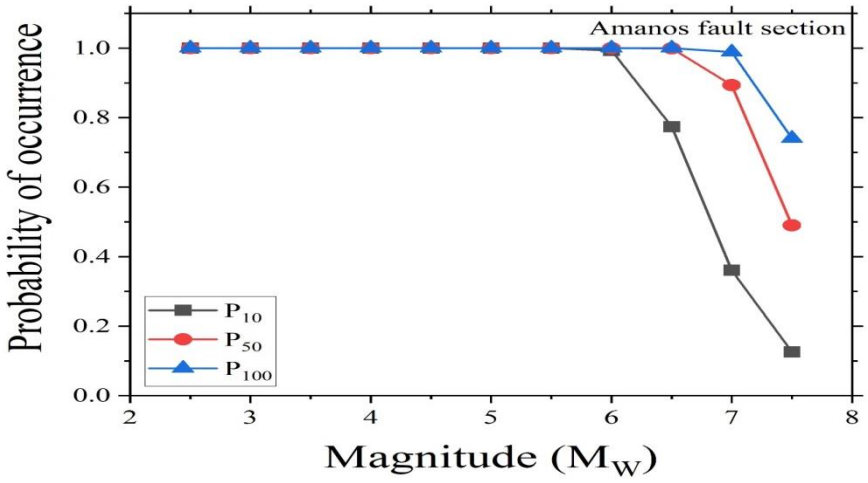

Figure 5.26: The probability of occurrences for Amanos fault section.

Using Equation 15 (as mentioned in chapter 2), we evaluated earthquake probabilities for the Pazarcık fault section over the next ten, fifty, and one hundred years. Table 5.15 shows a 100% probability for M_W 2.5 to 5.5 earthquakes within fifty years, and less than 50% for $M_W \geq 7.0$ earthquakes within one hundred years. [29] found a 0.92 probability for an M_S 5.0 earthquake in the next hundred years near the Pazarcık fault section. Our study found a 1.0 probability for an M_W 5.0 earthquake in the same period.

Table 5.15: The likelihood of occurrence of different earthquakes scaled at M_W scale for next 10, 50 and 100 years for the Pazarcık fault section.

Magnitude	**Pazarcık fault section**		
M_W	**P_{10}**	**P_{50}**	**P_{100}**
2.5	1	1	1
3.0	1	1	1
3.5	1	1	1
4.0	1	1	1
4.5	1	1	1
5.0	1	1	1
5.5	0.95888	1	1
6.0	0.55915	0.98335	0.99972
6.5	0.18959	0.65045	0.87781
7.0	0.05253	0.23645	0.41699
7.5	0.01375	0.0669	0.12932

Figure 5.27 illustrates the probability values for the Pazarcık fault section over the next hundred years.

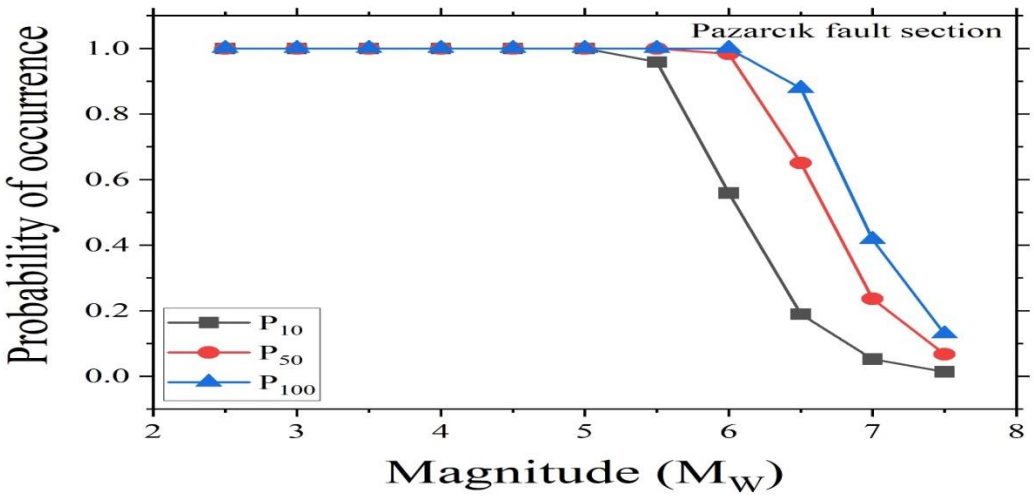

Figure 5.27: The probability of occurrences of earthquake in Pazarcık fault section.

Table 5.16 shows earthquake probabilities for the Erkenek fault section over the next ten, fifty, and one hundred years. Over the next hundred years, the probability for $M_W \leq 5.5$ earthquakes is over 50%, while for $M_W > 5.5$, it's under 50%. [29] reported a 1.0 probability for an M_S 5.0 earthquake in the next hundred years near the Erkenek fault section. Our study found a 0.79 probability for an M_W 5.5 earthquake in the same period.

Table 5.16: The likelihood of occurrence of different earthquakes scaled at M_W scale for next 10, 50 and 100 years for the Erkenek fault section.

Magnitude	**Erkenek fault section**		
M_W	**P_{10}**	**P_{50}**	**P_{100}**
2.5	1	1	1
3.0	1	1	1
3.5	1	1	1
4.0	1	1	1
4.5	0.99605	1	1
5.0	0.60491	0.99037	0.99991
5.5	0.14429	0.54119	0.78949
6.0	0.02581	0.12255	0.23008
6.5	0.00438	0.0217	0.04292
7.0	0.00074	0.00367	0.00733
7.5	0.00012	0.00062	0.00123

Additionally, the probability values for the Erkenek fault section over the next hundred years are illustrated in Figure 5.28.

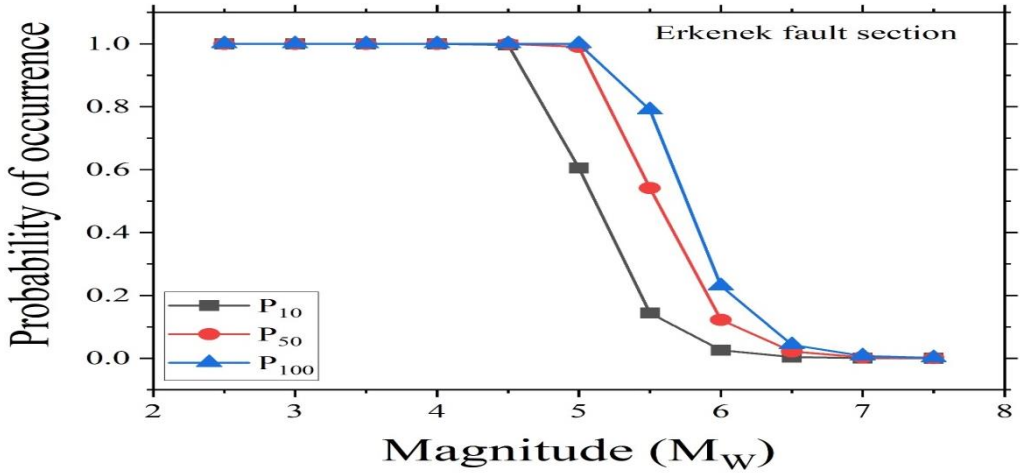

Figure 5.28: The probability of occurrences of earthquake in Erkenek fault section.

Table 5.17 shows the likelihood of earthquakes along the Çardak fault section over the next ten, fifty, and one hundred years. The second mainshock (M_W 7.6) occurred near this section. Within the next hundred years, earthquakes with $M_W \leq 5.5$ have a probability above 50%, while those with $M_W > 5.5$ have a probability below 50%. [29] noted a 1.0 probability for an M_S 5.0 earthquake in the next hundred years near Çardak. This study finds a 0.99 probability for an M_W 5.0 earthquake in the same period. Despite recent low activity, research by [30] and [31] indicates the potential for an M_W 7.0 or greater earthquake.

Table 5.17: The likelihood of occurrence of different earthquakes scaled at M_W scale for next 10, 50 and 100 years for the Çardak fault section.

Magnitude	**Çardak fault section**		
M_W	**P_{10}**	**P_{50}**	**P_{100}**
2.5	1	1	1
3.0	1	1	1
3.5	1	1	1
4.0	0.99999	1	1
4.5	0.94125	1	1
5.0	0.48566	0.964	0.9987
5.5	0.1444	0.54149	0.78977
6.0	0.03592	0.16716	0.30638
6.5	0.00854	0.042	0.08223
7.0	0.00201	0.01001	0.01993
7.5	0.00047	0.00236	0.00471

Additionally, the probability values for the Çardak fault section over the next hundred years are illustrated in Figure 5.29.

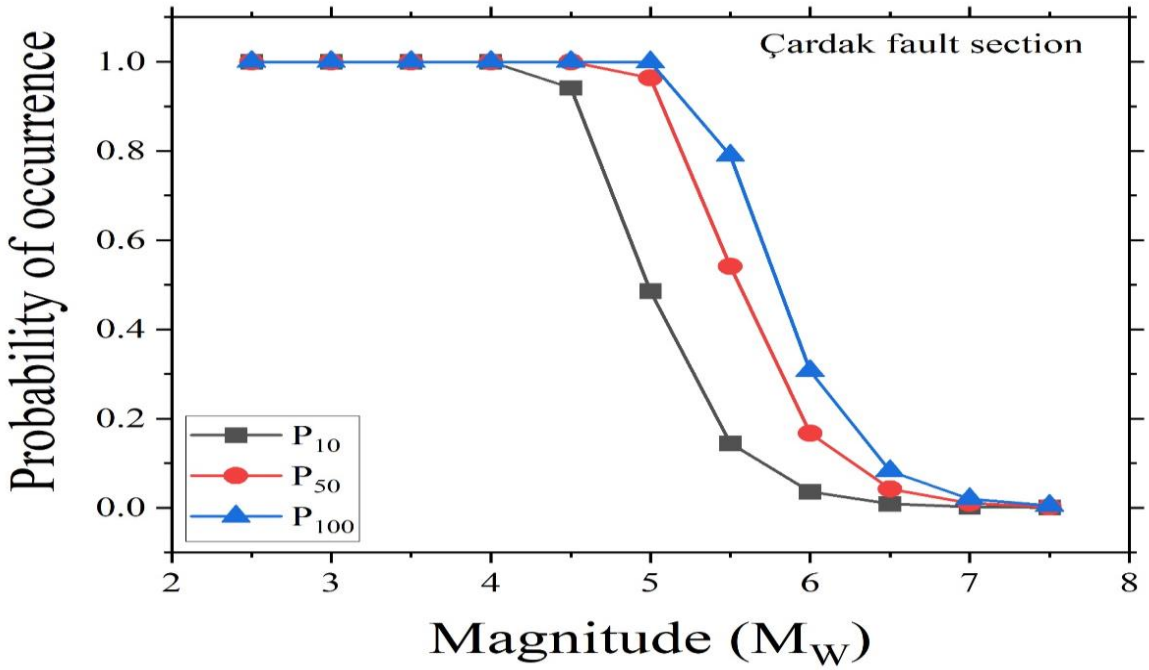

Figure 5.29: The probability of occurrences of earthquake in Çardak fault section.

5.5. Reference

[1] BIS. IS 1893 (part 1)–2002: Indian standard criteria for earthquake resistant design of structures, part 1 – general provisions and buildings. Bureau of Indian Standards, New Delhi (2002).

[2] Gumbel, E. J. Les valeurs extrêmes des distributions statistiques. *Annales de l'Institut Henri Poincaré* 5, 115–158 (1935).

[3] Gumbel, E. J. Statistics of extremes. Columbia University Press, New York (1958).

[4] Hazarika, D. and Kayal, J. R. Recent felt earthquakes (Mw 5.0–5.9) in Mizoram of north-east India region: Seismotectonics and precursor appraisal. G*eological Journal, 57(2): 877–885,* 2022.

[5] Sharma, S., Sarma, J. and Baruah, S. Dynamics of Mikir hills plateau and its vicinity: Inferences on Kopili and Bomdila Faults in North-eastern India through Seismotectonics, gravity, and magnetic anomalies. *Annals of Geophysics*, 61(3): p. SE338, 2018.

[6] Nath, S. K., Mandal, S., Das Adhikari, M. D. and Maiti, S. K. A unified earthquake catalogue for South Asia covering the period 1900–2014. *Natural Hazards*, 85(3): 1787–1810, 2017.

[7] Bora, D. K. Scaling relations of moment magnitude, local magnitude, and duration magnitude for earthquakes originated in Northeast India. *Earthquake Science,* 29(3): 153–164, 2016.

[8] Goswami, H. C. and Sarmah, S. K. A comparison of the estimated earthquake probabilities in the northeast Indian region. *Tectonophysics,* 95: 91–99, 1983.

[9] Rao, P. S. and Rao, B. R. Estimated earthquake probabilities in the northeast India and Andaman-Nicobar Island. *Mausam* 550.341.5, 267–273 (1979).

[10] Yadav, R. B. S., Tripathi, J. N., Shanker, D. et al. Probabilities for the occurrences of medium to large earthquakes in northeast India and adjoining region. *Natural Hazards,* 56: 145–167, 2011.

[11] Reasenberg, P. Second-order moment of central California seismicity 1969–1982. *Journal of Geophysical Research: Solid Earth,* 90(B7): 5479–5495, 1985.

[12] Barazangi, M., Sandvol, E. and Seber, D. Structure and tectonic evolution of the Anatolian plateau in eastern Turkey (2006).

[13] Tan, O. A homogeneous earthquake catalogue for Turkey. *Natural Hazards and Earth System Sciences,* 21(7): 2059–2073, 2021.

[14] Duman, T. and Emre, O. The East Anatolian Fault: geometry, segmentation and jog characteristics. *Geological Society, London, Special Publications,* 372(1):495–529, 2013.

[15] He, L. et al. Coseismic kinematics of the 2023 Kahramanmaras, Turkey earthquake sequence from InSAR and optical data. *Geophysical Research Letters,* 50: e2023GL104693, 2023.

[16] Tarı, U. et al. The geology and morphology of the Antakya Graben between the Amik Triple Junction and the Cyprus Arc. *Geodinamica Acta,* 26(1–2): 27–55, 2013.

[17] Alkan, H. et al. Seismic Hazard Implications in and Around the Yedisu Seismic Gap (Eastern Türkiye) Based on Coulomb Stress Changes, b-Values, and S-Wave Velocity. *Pure and Applied Geophysics,* 180: 3227–3248, 2023.

[18] Allen, C. R. Active faulting in northern Turkey. Div. Geol. Sci., Calif. Inst. Technol. Pasadena, Rep. 1577 (1969).

[19] Arpat, E. and Şaroğlu, F. Some observations and thoughts on the East Anatolian fault. *Bulletin of the Mineral Research and Exploration Institute of Turkey,* 73: 44–50, 1972.

[20] Güvercin, S. E., Karabulut, H., Konca, A. Ö., Doğan, U. and Ergintav, S. Active seismotectonics of the East Anatolian Fault. *Geophysical Journal International,* 230: 50–69, 2022.

[21] Uhrhammer, R. A. Characteristics of northern and central California seismicity. *Earthquake Notes* 57(1): 21, 1986.

[22] Tinti, S. and Mulargia, F. An improved method for the analysis of the completeness of a seismic catalogue. *Lettere al Nuovo Cimento*, 42: 21–27, 1985.

[23] Wiemer, S. and Wyss, M. Minimum magnitude of completeness in earthquake catalogs: Examples from Alaska, the Western United States, and Japan. *Bulletin of the Seismological Society of America*, 90(4): 859–869, 2000.

[24] Woessner, J. and Wiemer, S. Assessing the quality of earthquake catalogues: Estimating the magnitude of completeness and its uncertainty. *Bulletin of the Seismological Society of America*, 95(2): 684–698, 2005.

[25] Öztürk, S. Earthquake Hazard Potential in the Eastern Anatolian Region of Turkey: Seismotectonic b and Dc-Values and Precursory Quiescence Z-Value. *Frontiers in Earth Science,* 12 (1): 215–236, 2018.

[26] Bayrak, Y. et al. Seismogenesis and earthquake triggering during the Van (Turkey) 2011 seismic sequence. *Tectonophysics,* 601: 163–176, 2013.

[27] Maden, N. and Öztürk, S. Seismic B-values, Bouguer gravity and heat flow data beneath eastern Anatolia, Turkey: Tectonic implications. *Surveys in Geophysics*, 36(4): 549–570, 2015.

[28] Bora, D. K., Borah, K., Mahanta, R. and Borgohain, J. M. Seismic b-values and its correlation with Seismic Moment and Bouguer Gravity Anomaly over Indo-Burma Ranges of northeast India: Tectonic Implications. *Tectonophysics*, 728–729, 130–141 (2018).

[29] Bayrak, E. et al. Earthquake hazard analysis for East Anatolian fault zone, Turkey. *Natural Hazards,* 76(2): 1063–1077, 2015.

[30] Bayrak, Y. et al. Estimating earthquake hazard parameters from instrumental data for different regions in and around Turkey. *Engineering Geology,* 105: 200–210, 2009.

[31] Balkaya, M., Akyuz, H. S. and Özden, S. Paleoseismology of the Sürgü and Çardak faults - splays of the Eastern Anatolian Fault Zone, Türkiye. *Turkish Journal of Earth Sciences*, 32: 402–420, 2023.